

Position Sensorless Vector Control of Induction Motor including Field Weakening Mode of operation

A Project Report
Submitted in Partial Fulfilment of
Requirements for the Degree of
Master of Engineering
in
Electrical Engineering

By
Awneesh Kumar Tripathi



Department of Electrical Engineering
Indian Institute of Science
Bangalore - 560 012
India

June 2008

Acknowledgements

I feel a great pleasure in expressing my sincere thanks to Prof. V. T. Ranganathan who gave me a chance to work under his able guidance. His constant help, supervision and inspiration led me to complete the project in time. Course work dealt by him on electric drive was very helpful for the project.

I express my heartfelt gratitude to Prof. V. Ramanarayanan for his constant supervision and motivation during course work and project work. Course work dealt by him on SMPC and Power electronics was very helpful in understanding the fundamentals of the switched mode power conversion.

I sincerely thank Prof. G. Narayanan for his course work on digital controllers and PWM converters. I thank Prof. V. John for his encouragement and support during project.

I thank Prof. P. S. Nagendra Rao who was my adviser during my stay at IISc for his help and support. I thank Prof. D. Thukaram, Prof. Indraneel Sen and staff members of the department for their help and support.

I thank all senior PhD students of the PEG group Dinesh Gopinath, Kamalesh Hatua, Amit Jain, Debmalya Benerji for maintaining an excellent work culture in the lab and also taking me for two tours of Kerala and Karanataka.

I thank Tanmay, Dipankar De, Anirban, Shivaprasad, C. Karupuswamy, A. Karupuswamy, Parikshith, Pavan Hari, Chaitanya, Suneel, Bharat, Bhukia, Shravan, Anand Babu for their help and support. I thank Shilvi madam for her kind help and support.

I am grateful to MHRD for providing scholarship. I am grateful to IISc administration for providing it's students a very good working environment overall.

Abstract

DC motors were popularly used for variable speed applications until the advances in power electronics devices and digital electronics technology, as they require simple power processing unit and simple control algorithm and offer good dynamic performance. But conventional dc motor has problems related to mechanical commutation, while induction motor has low cost, less maintenance requirement, very rugged and reliable. So now induction motor drives run by voltage source inverters are replacing conventional dc motor drives in all variable speed applications.

In this project, attention is towards implementation of an induction motor drive suitable for traction application. As traction is a very high power application, switching losses will amount to a high value which can be minimized by using low switching frequency for the PWM inverter. Secondly traction system has very large inertia, so torque required during acceleration is many times higher the torque required during steady state full speed operation, because in steady state motor has to work only against air resistance and friction. So rather than using a very high power rating motor that can develop peak accelerating torque up to top speed, a smaller power rating motor can be used, which accelerates at limited constant power level, employing field weakening scheme.

Higher the voltage that can be applied to the motor, higher will be the flux in the core during field weakening operation and higher will be the torque capability. So inverter should be operated in over-modulation mode as well, extending to six step mode, to utilize dc bus voltage fully. Also for closed loop control, speed sensor is required which makes the motor costly, less reliable and less rugged, as it requires periodic maintenance. So position sensorless control is used, which uses the motor voltages and currents for speed and position synthesis.

Contents

Acknowledgements	i
Abstract	ii
List of Tables	vi
List of Figures	vii
Nomenclature	x
1 Introduction	1
1.1 Vector control	1
1.2 Special requirements of induction motor traction drive	3
1.3 Problems associated with vector control of induction motor traction drive . .	4
2 Schemes proposed for induction motor traction drive	5
2.1 Harmonic current extraction	5
2.1.1 Harmonic model of Induction motor	5
2.1.2 Extraction of fundamental current	6
2.1.3 Conclusion	8
2.2 Overmodulation scheme	9
2.2.1 Pulse dropping and Loss of volt-seconds	9
2.2.2 Redistributing commanded volt-seconds	9
2.2.3 Conclusion	13
2.3 Position sensorless scheme	13
2.3.1 Sensorless Principle	13

2.3.2	Stator Voltage Integration Problem	16
2.3.3	Removal of integration problem	17
2.3.4	Conclusion	19
2.4	Field weakeneing scheme	19
2.4.1	Voltage, current limits and optimum operating condition	19
2.4.2	Brief theory of the algorithm	21
2.4.3	Conclusion	22
3	Implementation	23
3.1	Introduction	23
3.2	Experimental Setup	23
3.2.1	Induction Motor-DC Generator Setup	23
3.2.2	Inverter Setup	26
3.2.3	FPGA Controller	27
3.3	Implementation	31
3.4	Estimation and calculation of different quantities	31
3.4.1	Base Values for Different Quantities	32
3.4.2	DC Bus Voltage Calculation	32
3.4.3	Sensed Voltage scaling	33
3.4.4	Sensed current scaling	33
3.4.5	Harmonic current extraction	33
3.4.6	Estimation of speed and position	33
3.4.7	Selection of K in flux position estimator block	36
3.4.8	Decoupling Circuit	36
3.5	Design and implementation of Controllers	37
3.5.1	General digital implementation of a controller	37
3.5.2	Design of Current Controller	38
3.5.3	Design of Speed Controller	39
3.5.4	Design of Flux Controller	39
3.5.5	Design of Voltage Controller	40
3.6	Conclusion	41

4	Experimental Results	42
4.1	Introduction	42
4.2	Current Extraction Waveforms	42
4.3	Overmodulation Waveforms	42
4.4	Steady State Waveforms	42
4.5	Transient Waveforms	48
4.6	Machine-2 Loading Waveforms	62
4.7	Conclusion	62
	References	64

List of Tables

3.1	Details of the induction motor	25
3.2	Parameters of the induction motor	26
3.3	Details of the DC generator	26
3.4	ALTERA FPGA device data	29
3.5	PU values	31
3.6	Base values	32
3.7	Controller parameters	41
4.1	Details of the induction motor-2	62

List of Figures

1.1	Block diagram of sensorless vector controlled induction motor drive	2
2.1	Block diagram for fundamental current extraction	7
2.2	Simulation result(fundamental current extraction)	8
2.3	Sine-Triangle PWM (Over-modulation)	10
2.4	Space-Vector PWM (Over-modulation, mode-1)	11
2.5	Space-Vector PWM (Over-modulation, mode-2)	11
2.6	Clamping level as a function of reference voltage peak(Sine-Triangle PWM) .	12
2.7	Clamping level as a function of reference voltage peak(Space-Vector PWM) .	12
2.8	Phasor diagram for rotor flux estimation	15
2.9	Block diagram for derivation of unit vectors $\cos\rho$ and $\sin\rho$	16
2.10	Modified unit-vector derieving algorithm block diagram	18
2.11	Voltage, current limits and optimum torque trajectory	20
2.12	Block diagram for field weakening algorithm	21
3.1	Block diagram for overall drive scheme	24
3.2	Experimental setup	25
3.3	Block diagram of FPGA board	28
3.4	Configuration of FPGA device	29
3.5	Block diagram of on-board clock network	30
3.6	Current loop	38
3.7	Speed loop	39
3.8	Flux loop	39
3.9	Voltage loop	40

4.1	V_{rn} and i_{sr} waveforms for speed command of $0.7pu$ ($35Hz$)	43
4.2	i_{rh} and i_{sr} (<i>extracted</i>) waveforms for speed command of $0.7pu$ ($35Hz$)	43
4.3	V_{rn} and i_{sr} waveforms for speed command of $0.92pu$ ($46Hz$)	44
4.4	i_{rh} and i_{sr} (<i>extracted</i>) waveforms for speed command of $0.92pu$ ($46Hz$)	44
4.5	V_{rn} and i_{sr} waveforms for speed command of $1.25pu$ ($64Hz$)	45
4.6	i_{rh} and i_{sr} (<i>extracted</i>) waveforms for speed command of $1.25pu$ ($64Hz$)	45
4.7	V_{ref} and V_{svpwm} (<i>modified</i>) waveforms for speed command of $0.75pu$ ($36Hz$)	46
4.8	V_{ref} and V_{svpwm} (<i>modified</i>) waveforms for speed command of $0.89pu$ ($44.5Hz$)	46
4.9	V_{ref} and V_{svpwm} (<i>modified</i>) waveforms for speed command of $0.94pu$ ($47Hz$)	47
4.10	V_{ref} and V_{svpwm} (<i>modified</i>) waveforms for speed command of $0.102pu$ ($50.6Hz$)	47
4.11	$\sin\rho$ and $\cos\rho$ waveforms for speed command of $0.0625pu$ ($3.125Hz$)	48
4.12	i_{s1} and i_{s2} waveforms for speed command of $0.0625pu$ ($3.125Hz$)	49
4.13	i_{sq} and i_{sd} waveforms for speed command of $0.0625pu$ ($3.125Hz$)	49
4.14	$\sin\rho$ and $\cos\rho$ waveforms for speed command of $0.75pu$ ($37.5Hz$)	50
4.15	i_{s1} and i_{s2} waveforms for speed command of $0.75pu$ ($37.5Hz$)	50
4.16	i_{sq} and i_{sd} waveforms for speed command of $0.75pu$ ($37.5Hz$)	51
4.17	$\sin\rho$ and $\cos\rho$ waveforms for speed command of $1.5pu$ ($75Hz$)	51
4.18	i_{s1} and i_{s2} waveforms for speed command of $1.5pu$ ($75Hz$)	52
4.19	i_{sq} and i_{sd} waveforms for speed command of $1.5pu$ ($75Hz$)	52
4.20	$\sin\rho$ and $\cos\rho$ waveforms for speed command of $2.25pu$ ($112.5Hz$)	53
4.21	i_{s1} and i_{s2} waveforms for speed command of $2.25pu$ ($112.5Hz$)	53
4.22	i_{sq} and i_{sd} waveforms for speed command of $2.25pu$ ($112.5Hz$)	54
4.23	Rotor reference and actual speed during transition from $0.75 pu$ ($37.5Hz$) to $1.5 pu$ ($75Hz$)	55
4.24	$\sin\rho$ and $\cos\rho$ during speed transition from $0.75 pu$ ($37.5Hz$) to $1.5 pu$ ($75Hz$)	55
4.25	V_{max} and V_{dq} during speed transition from $0.75 pu$ ($37.5Hz$) to $1.5 pu$ ($75Hz$)	56
4.26	i_{mr} (<i>reference</i>) and i_{mr} during speed transition from $0.75 pu$ ($37.5Hz$) to $1.5 pu$ ($75Hz$)	56
4.27	i_{sd} (<i>reference</i>) and i_{sd} during speed transition from $0.75 pu$ ($37.5Hz$) to $1.5 pu$ ($75Hz$)	57
4.28	i_{sq} (<i>reference</i>) and i_{sq} during speed transition from $0.75 pu$ ($37.5Hz$) to $1.5 pu$ ($75Hz$)	57
4.29	i_{s1} and i_{s2} during speed transition from $0.75 pu$ ($37.5Hz$) to $1.5 pu$ ($75Hz$)	58

4.30 Rotor reference and actual speed waveform during the speed reversal from 1.25 pu to -1.25 pu	58
4.31 $\sin\rho$ and $\cos\rho$ waveform during the speed reversal from 1.25 pu to -1.25 pu .	59
4.32 i_{s1} and i_{s2} waveform during the speed reversal from 1.25 pu to -1.25 pu . . .	59
4.33 V_{max} and V_{dq} waveform during the speed reversal from 1.25 pu to -1.25 pu . .	60
4.34 $i_{mr}(reference)$ and i_{mr} waveform during the speed reversal from 1.25 pu to -1.25 pu	60
4.35 $i_{sd}(reference)$ and i_{sd} waveform during the speed reversal from 1.25 pu to -1.25 pu	61
4.36 $i_{sq}(reference)$ and i_{sq} waveform during the speed reversal from 1.25 pu to -1.25 pu	61
4.37 i_{s1} and i_{s2} for speed command 1.25 pu (62.5 Hz) and load 129.2W	62
4.38 $i_{sq}(reference)$ and i_{sq} for speed command 1.25 pu (62.5 Hz) and load 129.2W	63

Nomenclature

Symbols : Definitions

V_{dc}	: DC bus voltage
v_{s1}, v_{s2}, v_{s3}	: 3-phase voltages applied on the induction motor
\underline{V}	: Voltage space phasor
v_{sa}, v_{sb}	: a-axis and b-axis components of \underline{V}
v_{sd}, v_{sq}	: d-axis and q-axis voltage components of \underline{V}
i_{s1}, i_{s2}, i_{s3}	: 3-phase line currents
\underline{i}_s	: Stator current phasor
i_{sa}, i_{sb}	: a-axis and b-axis components of \underline{i}_s
i_{sd}, i_{sq}	: d-axis and q-axis components of \underline{i}_s
i_{mr}	: Rotor magnetizing current
$\underline{\psi}_s$: Stator flux vector
ψ_{sa}, ψ_{sb}	: a-axis and b-axis components of $\underline{\psi}_s$
$\underline{\psi}_r^s$: Rotor flux phasor referred to stator coordinates
ψ_{ra}^s, ψ_{rb}^s	: a-axis and b-axis components of $\underline{\psi}_r^s$
ρ	: Position of the rotor flux phasor
ω_m	: Mechanical speed of the rotor in <i>rad/sec</i>
ω	: Electrical speed of the rotor in <i>rad/sec</i>
ω_1	: Speed of the rotor flux vector $\underline{\psi}_r$ or Stator frequency in <i>rad/sec</i>
ω_{slip}	: Slip frequency in <i>rad/sec</i>
ω^*	: Speed reference in <i>rad/sec</i>
i_{mr}^*	: Magnetizing current reference which corresponds to flux in the machine
i_{sd}^*, i_{sq}^*	: d-axis current and q-axis current references
$v_{s1}^*, v_{s2}^*, v_{s3}^*$: 3-phase reference modulating waves

\underline{V}^*	: Reference voltage phasor
v_{sa}^*, v_{sb}^*	: a-axis and b-axis components of \underline{V}^*
v_{sd}^*, v_{sq}^*	: d-axis and q-axis voltage components of \underline{V}^*
P	: number of poles
L_o	: mutual inductance between stator and rotor windings
L_{lr} or $\sigma_r L_o$: rotor leakage inductance
L_{ls} or $\sigma_s L_o$: stator leakage inductance
L_r	: rotor inductance
L_s	: stator inductance
R_r	: rotor resistance
R_s	: stator resistance
J	: moment of inertia of the motor
K_N	: proportional gain of the speed controller
T_N	: time constant of the speed controller
K_c	: proportional gain of the current controller
T_c	: time constant of the current controller
K_F	: flux controller gain constant
T_F	: flux controller time constant
K_v	: voltage controller gain constant
T_v	: voltage controller time constant
G	: gain of the converter
T_d	: delay of the converter
V_{max}	:voltage limit
I_{max}	: current limit
i_{mode2}	: field current's mode-2 condition value
I_{harm}	: harmonic motor current
m_L	: load torque(per unit)
T_r	: field time constant
T_w	: speed filter time constant
T_{dq}	: voltage filter time constant

Chapter 1

Introduction

The fact that the torque and speed in DC motor can be controlled independently by controlling armature current and field current respectively ensures that dc motor has good dynamic performance. The objective of vector control is to find two such components of currents from the available information of line currents of induction motor, by controlling which torque and speed can be controlled independently. This is the basic underlying principle of vector control which is most popular for induction motor drives.

1.1 Vector control

In case of induction motor, rotor flux rotates at the same speed as air gap flux separated by certain angle. By transforming the current space phasor in a synchronously rotating frame aligning rotor flux space phasor, we get two independent dc current components of the actual three phase current [4]. So vector control makes the control as simple and reliable as dc motor control. This is shown with equation 1.1, 1.2, 1.3, 1.4 and 1.5 here.

$$T_r \frac{di_{mr}(t)}{dt} + i_{mr}(t) = i_{sd}(t) \quad (1.1)$$

$$\omega_1(t) = \frac{d\rho}{dt} = \omega(t) + \frac{i_{sq}(t)}{T_r i_{mr}(t)} \quad (1.2)$$

$$M_d = \frac{2P}{3} \frac{L_0}{2(1+\sigma_r)} i_{mr}(t) i_{sq}(t) \quad (1.3)$$

$$R_s i_{sd}(t) + \sigma L_s \frac{di_{sd}}{dt} = v_{sd} + \sigma L_s \omega_1 i_{sq}(t) - (1-\sigma) L_s \frac{di_{mr}}{dt} \quad (1.4)$$

$$R_s i_{sq}(t) + \sigma L_s \frac{di_{sq}}{dt} = v_{sq} - \sigma L_s \omega_1 i_{sd}(t) - (1-\sigma) L_s \omega_1 i_{mr}(t) \quad (1.5)$$

For the purpose of the control, the d-axis and q-axis currents must be controlled independently. The presence of the terms containing i_{sq} in v_{sd} equation 1.4 and i_{sd} in v_{sq} equation 1.5 indicates cross coupling. Hence we need to add the following decoupling terms in the control circuit.

$$v_{sdx} = -\frac{\sigma L_s \omega_1 i_{sq}(t)}{G} + \frac{(1-\sigma)L_s \frac{di_{mr}}{dt}}{G} \quad (1.6)$$

$$v_{sqx} = \frac{\sigma L_s \omega_1 i_{sd}(t)}{G} + \frac{(1-\sigma)L_s \omega_1 i_{mr}(t)}{G} \quad (1.7)$$

where G is the gain of the inverter.

After adding the above mentioned components in the control circuit, the currents i_{sd} and i_{sq} , are completely decoupled and entirely depend upon the voltages v_{sd} and v_{sq} respectively as shown in equations 1.8 and 1.9.

$$R_s i_{sd}(t) + \sigma L_s \frac{di_{sd}}{dt} = v_{sd} \quad (1.8)$$

$$R_s i_{sq}(t) + \sigma L_s \frac{di_{sq}}{dt} = v_{sq} \quad (1.9)$$

This is shown in the block diagram 1.1.

1.2 Special requirements of induction motor traction drive

1. Switching losses are directly proportional to switching frequency. So in traction application (MW power level), low switching frequency (less than 1 KHz) inverter operation is required to reduce switching device heating.
2. Traction system has large inertia, so torque required during acceleration is very high compared to steady state operation. If field weakening mode of operation is followed, motor power rating can be saved.
3. Overmodulation operation leading to six step mode operation of the inverter, produces maximum possible stator voltage out of limited DC bus voltage which is required for maximum torque production.
4. Position sensor (optical or magnetic) makes induction motor expensive and less reliable, so a position sensorless vector control is preferable.

1.3 Problems associated with vector control of induction motor traction drive

1. Low switching frequency PWM operation and over modulation operation will result in high stator current ripple. So d-q frame currents required by vector control will be distorted and good control can not be possible. If one puts a heavy filter it will slow the current loop too much. So some suitable current extraction algorithm has to be followed.
2. DC bus voltage has to be utilized for maximum torque production, but as the reference goes above triangle carrier peak, pulse dropping occurs and linearity between input reference and output voltage is lost. So suitable compensation has to be applied.
3. Flux position is estimated by integration of applied stator excitation voltage. Pure integration leads to saturation so first order filter is used instead, but at low speed this creates problem because of relatively wrong position estimate. So this needs to be improved.
4. Field weakening has to be done in such a manner that accelerating torque follows maximum torque trajectory without violating either current limit or voltage limit. So suitable algorithm is needed here as well.

In the next chapter, proposed solutions to the above discussed problems are presented.

Chapter 2

Schemes proposed for induction motor traction drive

2.1 Harmonic current extraction

As mentioned earlier we are operating the inverter at low switching frequency and in over-modulation mode as well as normal mode. This is adopted to make switching losses small and utilize the available DC bus voltage fully. PWM output voltage is pure sine wave if switching frequency is infinite and inverter operates in normal mode. As we are violating both constraints, actual PWM output voltage has considerable harmonics which will produce larger harmonic current, since for harmonics, the induction motor behaves as leakage inductance load only. This distorted current has to be used by speed estimation block and current controller. So system has a very high risk of instability. If we put a low pass filter to correct the problem, it becomes worse because of the delay introduced by the filter. In this chapter we present a different approach to extract fundamental current [2, 7].

2.1.1 Harmonic model of Induction motor

We have voltage and flux equations as follows

$$\underline{v}_s^s = R_s \underline{i}_s^s + \frac{d\underline{\psi}_s^s}{dt} \quad (2.1)$$

$$\underline{v}_r^s = R_r \underline{i}_r^s + \frac{d\underline{\psi}_r^s}{dt} \quad (2.2)$$

$$\underline{\psi}_s^s = L_s \underline{i}_s^s + L_0 \underline{i}_r^r e^{j\varepsilon} \quad (2.3)$$

$$\underline{\psi}_r^s = L_r \underline{i}_r^r e^{j\varepsilon} + L_0 \underline{i}_s^s \quad (2.4)$$

Virtually no current flows through magnetizing inductance for harmonic frequency and leakage inductance being small, we can neglect rotor flux linkage term in equation 2.2. From equations 2.1, 2.2, 2.3 and 2.4, we derive

$$\underline{v}_s^s = R_s \underline{i}_s^s + L_s \frac{d\underline{i}_s^s}{dt} + L_0 \left[\frac{d\underline{i}_r^r}{dt} e^{j\varepsilon} + j\omega \underline{i}_r^r \right] \quad (2.5)$$

$$\underline{v}_r^s = 0 = R_r \underline{i}_r^s + \frac{d\underline{\psi}_r^s}{dt} - j\omega \underline{\psi}_r^s \quad (2.6)$$

And from equations 2.5 and 2.6, we get

$$\underline{v}_s^s = R_s \underline{i}_s^s + L_s \frac{d\underline{i}_s^s}{dt} - \frac{L_0}{L_r} [R_r \underline{i}_r^r e^{j\varepsilon} + L_0 \frac{d\underline{i}_s^s}{dt}] \quad (2.7)$$

Neglecting rotor flux in equation from 2.4, we get $\underline{i}_r^r e^{j\varepsilon} = -\frac{L_0}{L_r} \underline{i}_s^s$. By substituting this expression in equation 2.7, we get

$$\underline{v}_s^s = [R_s + R_r \left(\frac{L_0}{L_r}\right)^2] \underline{i}_s^s + \sigma L_s \frac{d\underline{i}_s^s}{dt} \quad (2.8)$$

or

$$v_h = R_h i_h + L_h \frac{di_h}{dt} \quad (2.9)$$

Here $L_h = \sigma L_s$ and $R_h = [R_s + R_r \left(\frac{L_0}{L_r}\right)^2]$. This equation 2.9 describes the harmonic model of induction motor.

2.1.2 Extraction of fundamental current

First we calculate the harmonic voltage by subtracting weighted reference voltage (pure sine wave) from actual PWM output voltage. Now this harmonic voltage is applied as input to the induction motor harmonic model which produces harmonic current as output. This harmonic current has to be subtracted from actual induction motor current to get fundamental motor current. This is shown with block diagram 2.1. Also it is to be noted that at low switching frequency, fundamental inverter output voltage is lower than what it is expected to be. So after deduction of weighted reference from it, the assumed harmonic voltage, actually has some negative fundamental voltage also. This produces large negative fundamental current from the harmonic model which presents low impedance to fundamental voltage. After deduction of it from actual motor current, fundamental current estimated is actually higher than the real fundamental current. This causes the current limit to over-act and hence motor can not accelerate at the maximum possible rate. For compensation, estimated harmonic

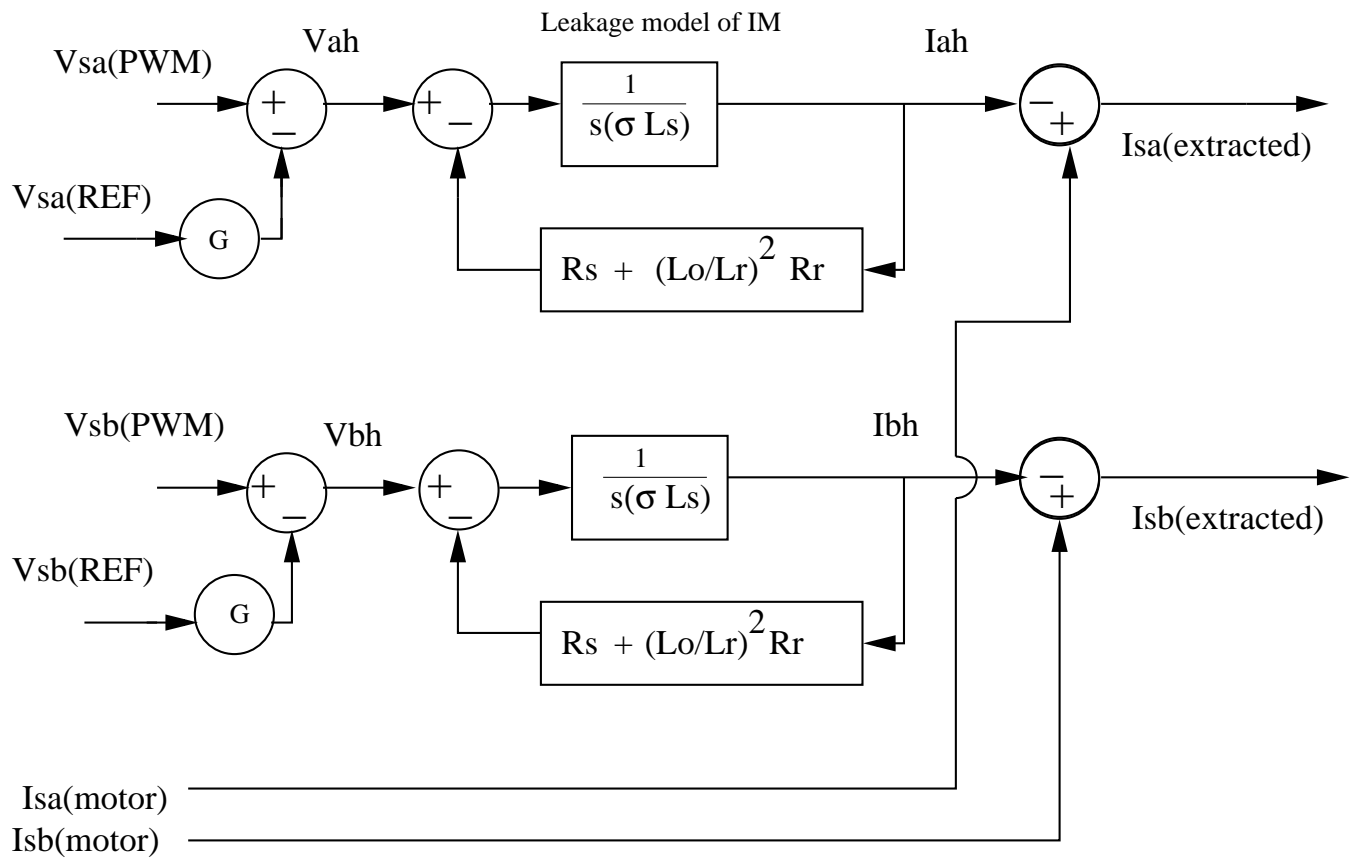


Figure 2.1: Block diagram for fundamental current extraction

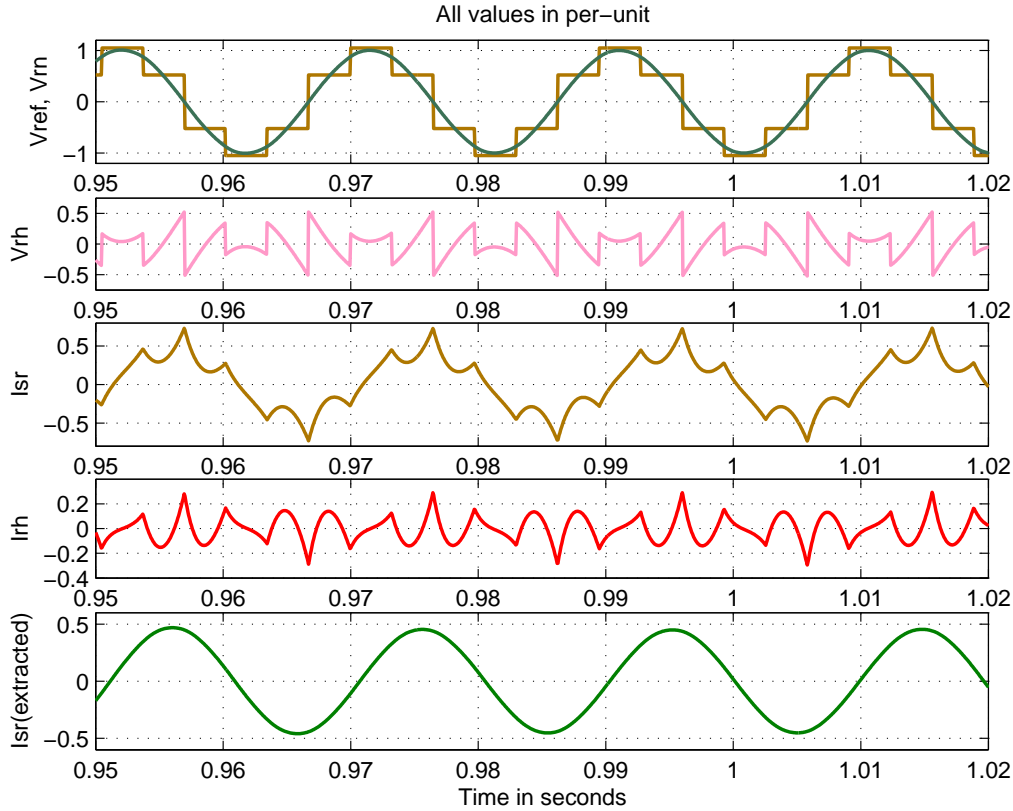


Figure 2.2: Simulation result(fundamental current extraction)

current should be converted into d-q components, which should be passed through high pass filters to remove the dc component (fundamental current in a-b-c), then converted back to stator frame and subtracted from the motor current to get the fundamental current. A simulation output is shown in figure 2.2.

2.1.3 Conclusion

This algorithm has been tested on Simulink/Matlab and also verified on experimental set up. Here we avoid use of a heavy filter, so there is no danger to stability of the system. Extracted current is pure sinusoidal, however it depends on correctness of the machine parameters. So $d - q$ components are pure DC quantities which are fed to current controller. Extracted fundamental current and sinusoidal reference voltage are fed to flux position estimator which produces ρ and $\sin\rho, \cos\rho$ as output.

2.2 Overmodulation scheme

DC bus voltage is limited to lower value in traction application due to economical constraints, for example cost of bus insulators and cost of switching devices and motor. The maximum fundamental three phase ac voltage that can be generated from it occurs when inverter operates in six step mode. But in any PWM technique, when reference voltage exceeds the triangular carrier amplitude (modulation index > 1.0 for sine-triangle PWM and modulation index $> \frac{2}{\sqrt{3}}$ for Space-vector PWM and triplen harmonics injection PWM), the output gets saturated and the linearity between output voltage and reference voltage is lost. This causes the actual gain of the inverter to be lower than that expected by closed loop controller, so overall drive performs poorly. To compensate for drop in gain in over-modulation region, some methods have been in practice. In one of the methods, reference is modified by clamping it at high or low depending on polarity and maintaining quarter wave symmetry, at certain angle which is decided by modulation index of the reference [1]. The angle is calculated such that the modified reference (fundamental magnitude) becomes equal to actual reference magnitude.

2.2.1 Pulse dropping and Loss of volt-seconds

In a PWM algorithm, input reference voltage is compared to triangular switching frequency wave; when the reference exceeds triangle wave value, output pulse is high, otherwise low. At the maximum, high can occur for full sampling duration when the input reference magnitude is equal or greater than the triangle peak magnitude. So the reference magnitude greater than the triangle peak magnitude, produces saturated average output. So there is a loss of volt-seconds in the pulse dropping region. Below it is shown with help of figures 2.3, 2.4 and 2.5

2.2.2 Redistributing commanded volt-seconds

In order to maintain linearity between reference voltage and inverter output voltage, volt-seconds lost due to PWM saturation is compensated by adding extra volt-seconds in reference voltage itself [1]. This is done by clamping the original command to $+1$ or -1 per unit for a portion of the cycle. The duration for which this clamping takes place is calculated such that per unit reference fundamental voltage becomes equal to per unit output fundamental

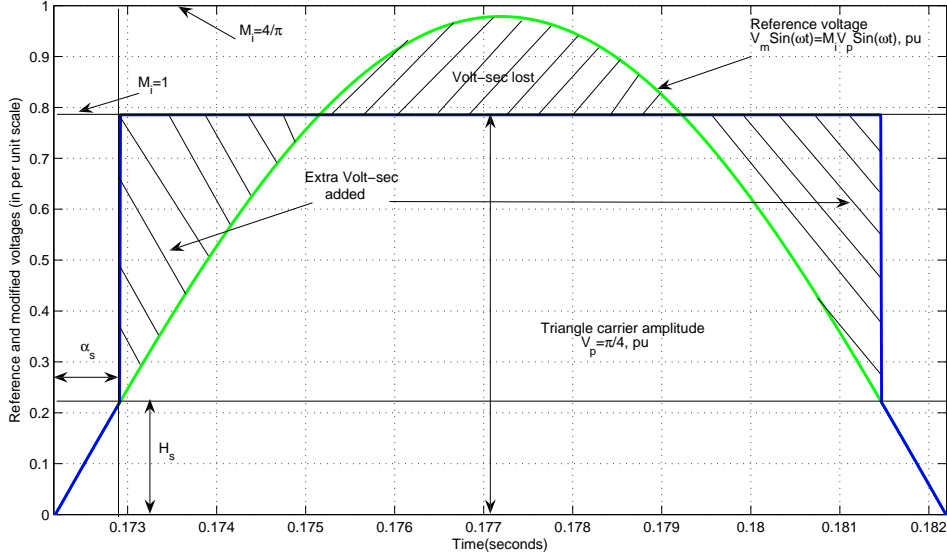


Figure 2.3: Sine-Triangle PWM (Over-modulation)

voltage. This is shown with figures 2.3, 2.4 and 2.5. For sine-triangle we have following relations:

$$H_s = V_m \sin(\alpha_s) \quad (2.10)$$

$$V_m = \cos(\alpha_s) + \frac{V_m}{\pi} [2\alpha_s - \sin(2\alpha_s)] \quad (2.11)$$

Equations 2.10 and 2.11 are valid for full over-modulation range ($1 \leq M_i \leq \frac{4}{\pi}$). For space vector PWM, there are two modes of operation in over-modulation region. In the first mode, clamping has to be done at two peaks per half cycle because of the wave shape and in second mode clamping is done once per half cycle as reference gets more saturated and clamping requirement is more. The equations for first mode are 2.12 and 2.13.

$$H_{sv} = \frac{V_m}{4} [3\sin(\alpha_{sv}) + \sqrt{3}\cos(\alpha_{sv})] \quad (2.12)$$

$$V_m = \frac{1}{\pi} \left[-\frac{3}{4} V_m \sin(2\alpha_{sv}) + 3V_m \alpha_{sv} - \frac{3\sqrt{3}}{4} V_m \cos(2\alpha_{sv}) + \frac{3\pi}{2} \cos(\alpha_{sv}) - \sqrt{3} \frac{\pi}{2} \sin(\alpha_{sv}) \right] \quad (2.13)$$

And for second mode of operation, the equations are 2.14 and 2.15.

$$H_{sv} = \frac{3}{2} V_m \sin(\alpha_{sv}) \quad (2.14)$$

$$V_m = \frac{1}{\pi} \left[-\frac{3}{2} V_m \sin(2\alpha_{sv}) + 3V_m \alpha_{sv} + \pi \cos(\alpha_{sv}) \right] \quad (2.15)$$

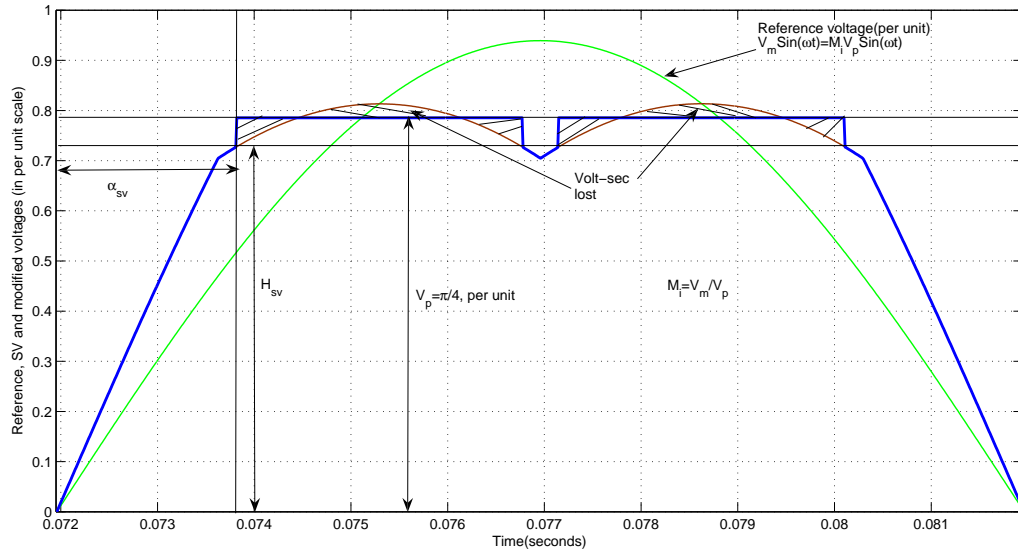


Figure 2.4: Space-Vector PWM (Over-modulation, mode-1)

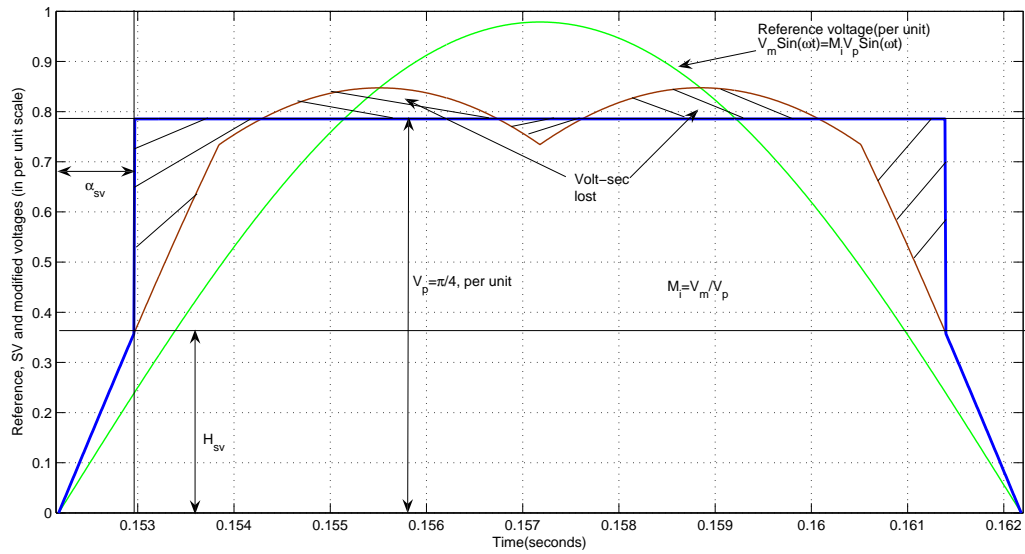


Figure 2.5: Space-Vector PWM (Over-modulation, mode-2)

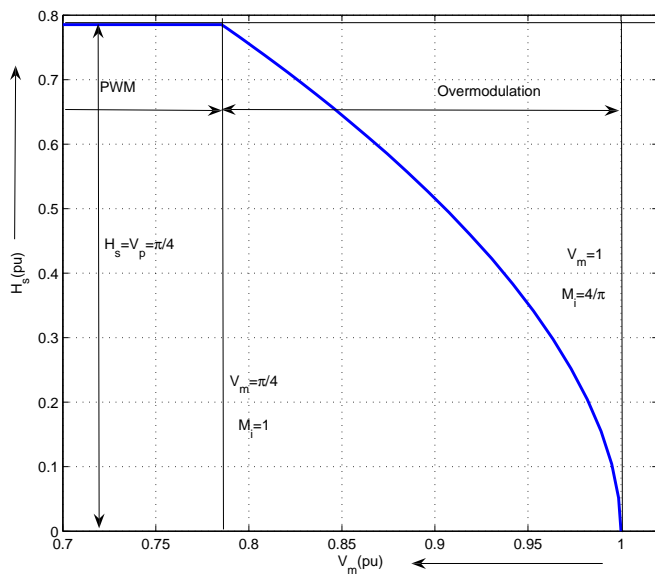


Figure 2.6: Clamping level as a function of reference voltage peak(Sine-Triangle PWM)

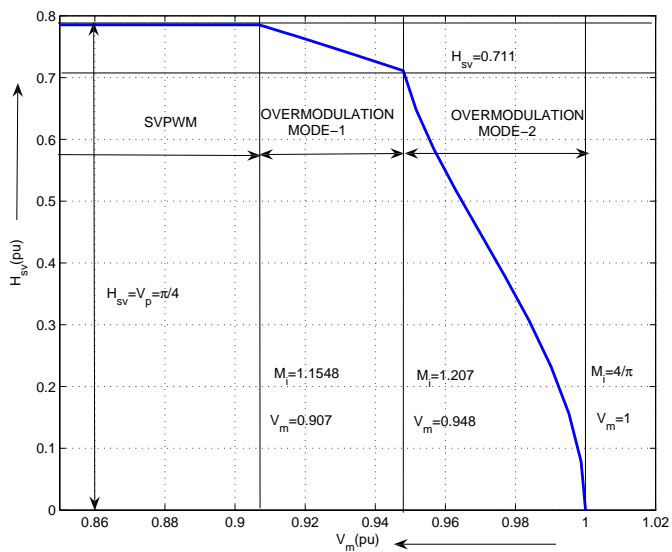


Figure 2.7: Clamping level as a function of reference voltage peak(Space-Vector PWM)

Based on these equations lookup table can be constructed which takes modulation index M_i as input and gives H_s or H_{sv} value as output. It is shown with graphs 2.6 and 2.7. A comparator clamps input reference command to $+1$ or -1 per unit with input polarity, if its magnitude exceeds H_s or H_{sv} value. The algorithm is here

$$\begin{aligned} V_{PWM*} &= V_{PWM}, [when \quad -H_{PWM} = < V_{PWM} = < H_{PWM}] \\ &= \text{sign}(V_{PWM}), [otherwise] \end{aligned} \quad (2.16)$$

2.2.3 Conclusion

Space vector is better than sine-triangle PWM as it remains linear upto modulation index of $\frac{2}{\sqrt{3}}$. In fact in space vector PWM, triplen harmonics(*third harmonics* = $\frac{1}{3}$, *maximum*, *ninth harmonics* = $\frac{1}{9}$, *maximum*) are injected to increase output fundamental voltage, which are inherently canceled by balanced three phase system. But to increase fundamental volatge further one has to inject 5, 7, 11, 13.. harmonics also, all the way upto six step or square wave mode. That's what we are doing here indirectly [1].

2.3 Position sensorless scheme

In field oriented control, a rotational transducer such as tachometer, or an encoder or a resolver, is mounted on the induction motor shaft. However, a speed sensor can not be mounted on a shaft in some cases, such as motor drives in hostile environment or high speed motor drives. Further, these sensors suffer from low reliability, high cost and noise. Therefore, sensorless drives are increasingly employed in modern industrial applications. The advantages of speed sensorless induction motor drives are lower cost, elimination of sensor cable (which is prone to noise signals) and increased reliability. In this section, the principle of sensorless operation, the algorithm employed to estimate the rotor flux position and the speed, and the practical problems and constraints involved, and their solution are presented [5].

2.3.1 Sensorless Principle

The rotor speed in elec-rad/sec(ω) , rotor flux speed (ω_1) and the slip frequency(ω_{slip}) can be related as follows,

$$\omega = \omega_1 - \omega_{slip}$$

In this section the equations required for the determination of the rotor flux speed (ω_1) are developed and as explained in previous chapters, slip frequency (ω_{slip}) is given by $\omega_{slip} = \frac{i_{sq}}{T_r i_{mr}}$. Thus the rotor speed (ω) is estimated which is used as feed back quantity in the speed loop.

The stator and rotor flux linkages in terms of the stator and rotor currents can be expressed as follows,

$$\underline{\psi}_s^s = L_s \underline{i}_s^s + L_0 \underline{i}_r^r e^{j\varepsilon} \quad (2.17)$$

$$\underline{\psi}_r^r = L_r \underline{i}_r^r + L_0 \underline{i}_s^s e^{-j\varepsilon} \quad (2.18)$$

Referring the rotor flux in stationary coordinate system,

$$\underline{\psi}_r^s = \underline{\psi}_r^r e^{j\varepsilon} = L_r \underline{i}_r^r e^{j\varepsilon} + L_0 \underline{i}_s^s \quad (2.19)$$

From equations (2.17), (2.19) the rotor current referred to the stator can be expressed as in equation (2.20)

$$\underline{i}_r^r e^{j\varepsilon} = \frac{\underline{\psi}_r^s - L_0 \underline{i}_s^s}{L_r} \quad (2.20)$$

Substituting this value from equation 2.20 in equation 2.17 we get

$$\begin{aligned} \underline{\psi}_s^s &= [L_s \underline{i}_s^s + \frac{L_0}{L_r} (\underline{\psi}_r^s - L_0 \underline{i}_s^s)] \\ \underline{\psi}_r^s &= \frac{L_r}{L_0} (\underline{\psi}_r^s - \sigma L_s \underline{i}_s^s) \end{aligned} \quad (2.21)$$

where $\sigma = 1 - \frac{L_0^2}{L_s L_r}$

Therefore rotor flux referred to the stator can be written as shown in Eqn. 2.21.

The stator voltage equation in space phasor form can be written as follows which can be used for the calculation of the stator flux.

$$\underline{v}_s^s = R_s \underline{i}_s^s + \frac{d\underline{\psi}_s^s}{dt} \quad (2.22)$$

From the above equation (2.22) the stator flux linkages can be expressed as,

$$\underline{\psi}_s^s = \int (\underline{v}_s^s - R_s \underline{i}_s^s) dt \quad (2.23)$$

From equations (2.23), (2.21), the rotor flux is calculated

$$\underline{\psi}_r^s = \frac{L_r}{L_0} [(\int (\underline{v}_s^s - R_s \underline{i}_s^s) dt) - \sigma L_s \underline{i}_s^s] \quad (2.24)$$

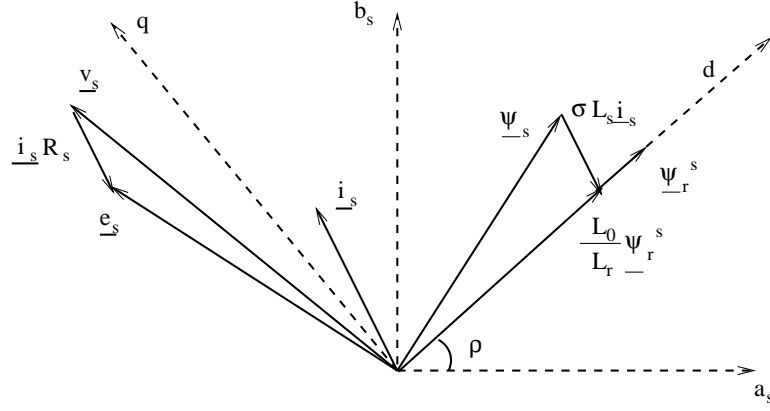


Figure 2.8: Phasor diagram for rotor flux estimation

The relationship between the stator flux and rotor flux can be shown in a phasor diagram as shown in Fig. 2.8. The rotor flux phasor is expressed in stationary coordinates as,

$$\underline{\psi}_r^s = \psi_{ra}^s + j\psi_{rb}^s$$

The rotor flux linkage phasor is normalized to get sine and cosine of the rotor flux angle, which is used for resolving stator reference frame phasors to rotor flux reference frame or vice versa. The following equations show the normalization to obtain the unit vectors $\cos\rho$ and $\sin\rho$. This is shown in Fig. 2.9 in the form of a block diagram.

$$\begin{aligned} \cos\rho &= \frac{\psi_{ra}^s}{|\psi_r^s|} \\ \sin\rho &= \frac{\psi_{rb}^s}{|\psi_r^s|} \end{aligned} \quad (2.25)$$

where $|\psi_r^s| = \sqrt{\psi_{ra}^s{}^2 + \psi_{rb}^s{}^2}$. The rotor flux speed with respect to stationary reference frame is estimated using the relation,

$$\omega_1 = \frac{d\rho}{dt} \quad (2.26)$$

By simple mathematics, it can be seen that

$$\frac{d\theta}{dt} = \cos\theta \frac{d}{dt}(\sin\theta) - \sin\theta \frac{d}{dt}(\cos\theta)$$

Hence the speed of the rotor flux can be expressed as follows,

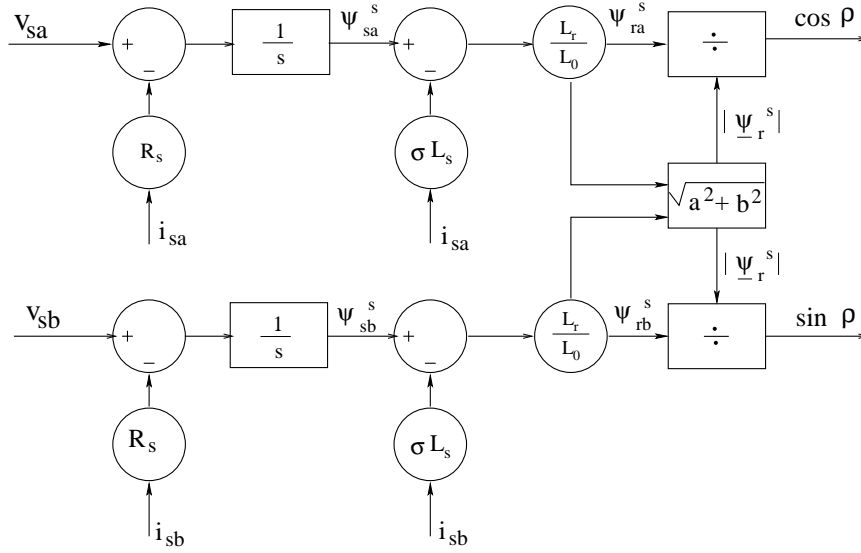


Figure 2.9: Block diagram for derivation of unit vectors $\cos\rho$ and $\sin\rho$

$$\omega_1 = \frac{d\rho}{dt} = \cos\rho \frac{d}{dt}(\sin\rho) - \sin\rho \frac{d}{dt}(\cos\rho) \quad (2.27)$$

Therefore, the rotor speed(ω) in elec-rad/sec is,

$$\omega = \omega_1 - \omega_{slip} \quad (2.28)$$

where $\omega_{slip} = \frac{i_{sq}}{T_{rimr}}$

2.3.2 Stator Voltage Integration Problem

Flux estimation is an important task in implementing sensorless algorithm, because of the fact, that the unit vectors, used for transforming the quantities from stationary coordinate system to rotating frame of reference depend on the flux estimation. Integrating back emf in the machine leads to the flux estimation. The only parameter required is stator winding resistance, which can be easily obtained in most cases and in most of the cases can be considered constant. Hence this method is much preferred than estimation of stator flux from stator currents.

However there are practical problems involved in the realization of a pure integrator. Hence motor flux estimation is no easy task. A pure integrator has a dc drift and initial

value problems. A dc component in measured motor back emf is inevitable in practice. This dc component, no matter how small it is, can finally drive the pure integrator into saturation. If initial value is not selected properly, a constant dc offset will appear at the output. This offset, representing a constant dc flux in a motor, does not exist during motor normal operation. A common solution to these problems is to replace the pure integrator with a first order low pass filter [6].

$$\underline{\psi}_s^s = \frac{1}{s + \omega_0} \underline{e}_s^s \quad (2.29)$$

where ω_0 is the filter cut off frequency. By choosing ω_0 to be very small, the integrator well approximates to a pure integrator. Therefore it can be seen that small amount of negative feedback is required to maintain the stability of the integrator in the presence of noise or offset errors.

This ω_0 can't be selected too small otherwise dc offset will decrease slowly during transients and drive might become unstable. So the drive performs satisfactorily at higher speed but it becomes unstable at lower speed because of inaccurate position and speed estimation.

2.3.3 Removal of integration problem

So we can't approximate a pure integrater by a low pass filter because of the reasons discussed above. But some fast error decaying mechanizm must be employed to ensure that there is no dc offset. For this we need one more estimate of rotor flux. We know that i_{mr} represents rotor flux equivalent current, so $L_0 i_{mr}$ represents magnitude of rotor flux and $e^{j\rho}$ is its position with respect to stator. So we can calculate rotor flux error and add it to the integrator input after multiplying with some gain K . It is shown with equation 2.30 and figure 2.10.

$$\underline{\psi}_r^{s*} = L_0 i_{mr} e^{j\rho}$$

$$\underline{\psi}_s^s = \int [(\underline{v}_s^s - R_s \underline{i}_s^s) + K(\underline{\psi}_r^{s*} - \underline{\psi}_r^s)] dt \quad (2.30)$$

The value of K decides how fast error converges to zero. If we select a very high value of K , their exists a starting problem though once started drive behaves ideally, and smaller value of K gives poor steady state performance. So K is selected on trial basis here. This method promises accurate position and speed estimation, right from 1% to any higher speed.

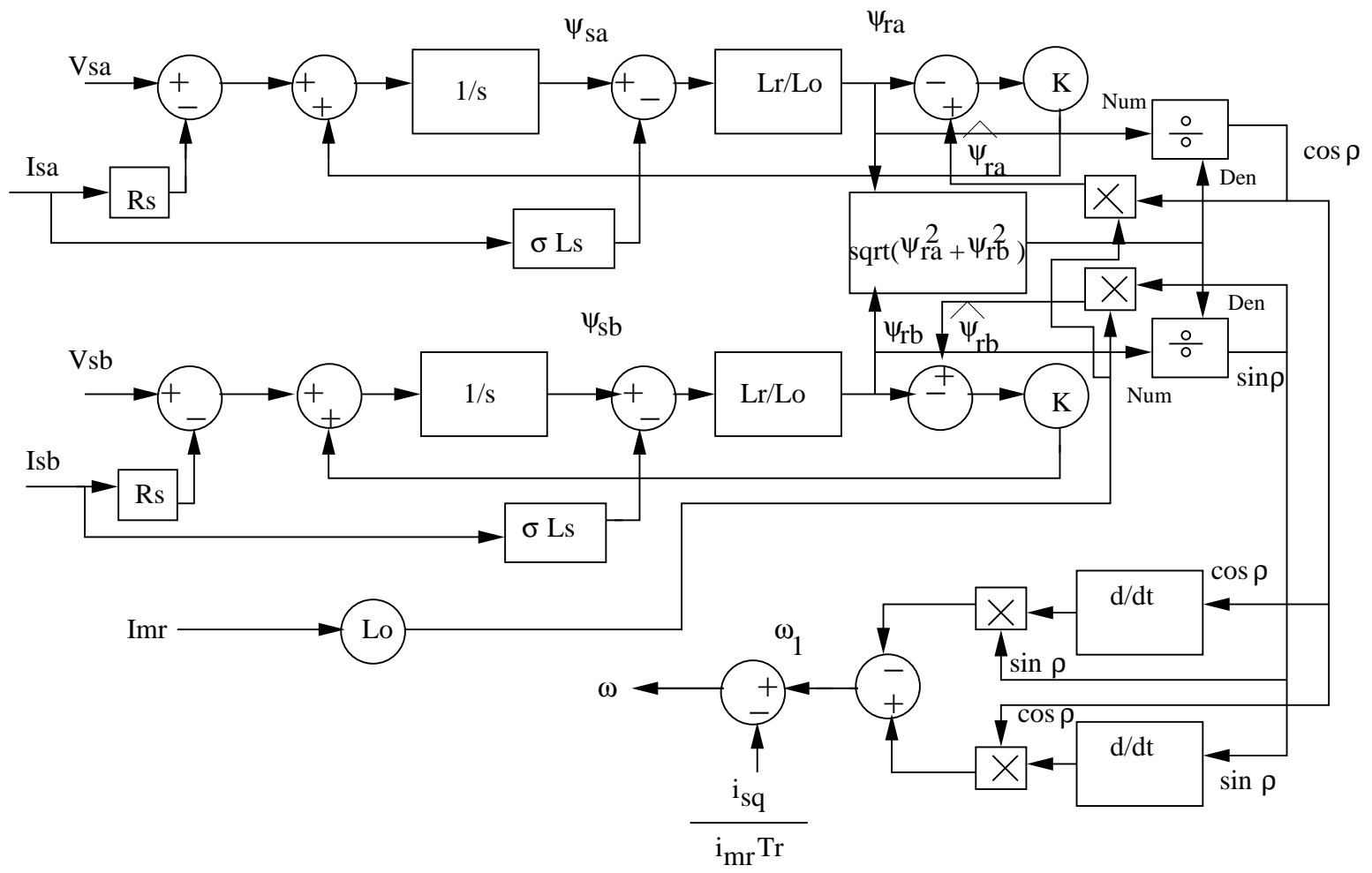


Figure 2.10: Modified unit-vector deriving algorithm block diagram

2.3.4 Conclusion

This algorithm has been tested on Simulink/Matlab and also verified on experimental set up. This gives very good performance compared to low pass filter integration method.

2.4 Field weakening scheme

As discussed earlier in the report that, a smaller power rating motor which accelerates at constant power level above rated speed to achieve full speed, can be used in traction application for better utilization of resources. This can be achieved by a proper field weakening algorithm which must also ensure optimum utilization of DC bus voltage. As DC bus voltage is the major limiting factor of maximum torque capability in field weakening mode of operation, in this section, a proper algorithm for field weakening operation is discussed [3, 5].

2.4.1 Voltage, current limits and optimum operating condition

The maximum fundamental phase voltage that can be achieved from the inverter with DC bus voltage V_{dc} is $\frac{2V_{dc}}{\pi}$ in six step mode. So we have $V_{max} = \frac{3V_{dc}}{\pi} \geq \sqrt{V_{sd}^2 + V_{sq}^2}$, as the voltage limit. Here we can do some approximation as follows in equation 1.4 and 1.5.

$$V_{sd} = -\omega_1 \sigma L_s i_{sq} \quad (2.31)$$

and

$$V_{sq} = \omega_1 L_s i_{sd} \quad (2.32)$$

So from above equations we get voltage limit ellipse equation as follows

$$\frac{i_{sd}^2}{\left(\frac{V_{max}}{\omega_1 L_s}\right)^2} + \frac{i_{sq}^2}{\left(\frac{V_{max}}{\sigma \omega_1 L_s}\right)^2} = 1 \quad (2.33)$$

As maximum current is also limited, we have equation of a circle as follows

$$i_{sd}^2 + i_{sq}^2 = i_{max}^2 \quad (2.34)$$

Now the operating point must always be inside the region limited by both the boundaries. The equation for torque is given by

$$M_d = \frac{2P}{3} \frac{L_0}{2(1 + \sigma_r)} [i_{sd}(t) i_{sq}(t)] \quad (2.35)$$

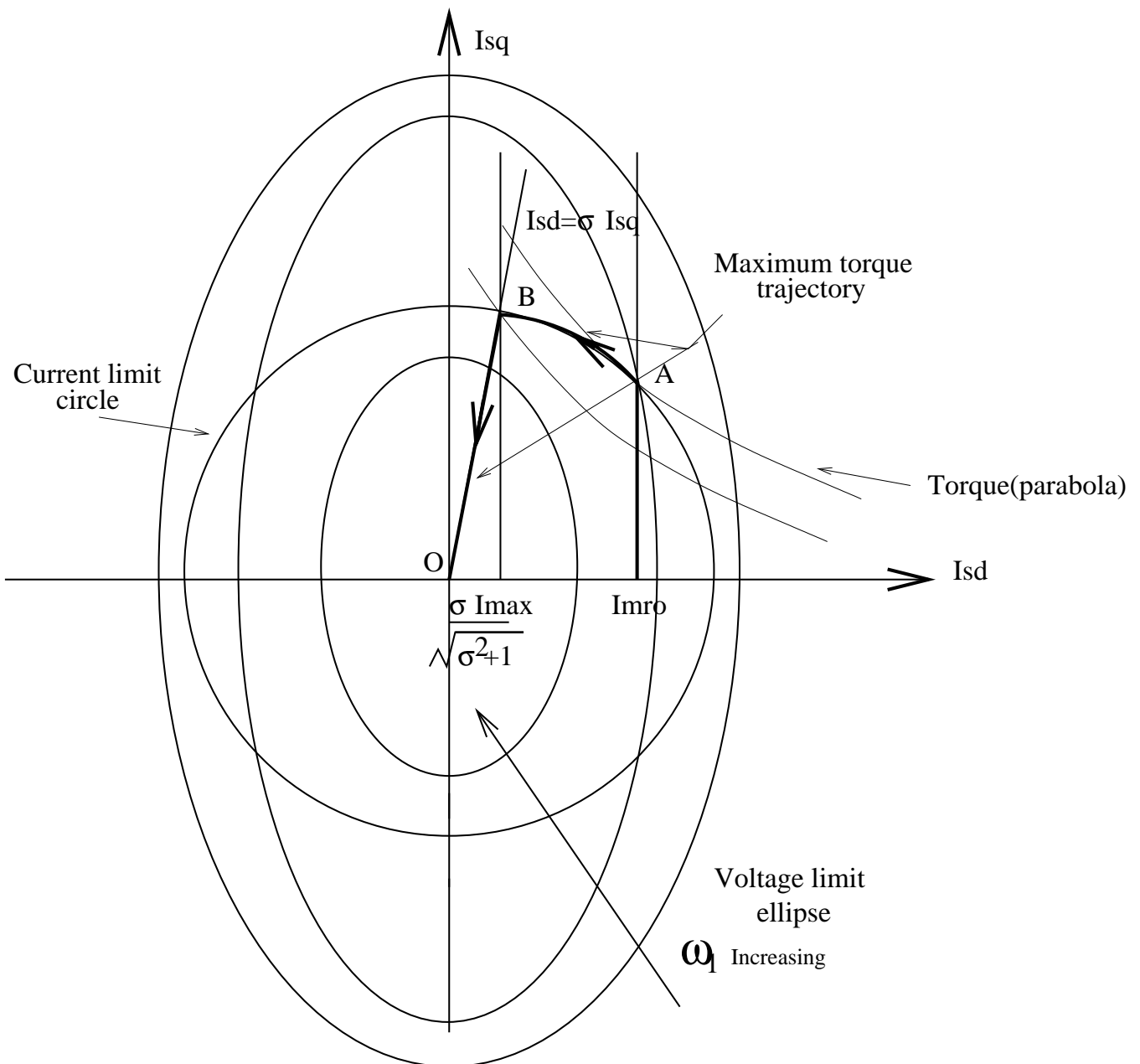


Figure 2.11: Voltage, current limits and optimum torque trajectory

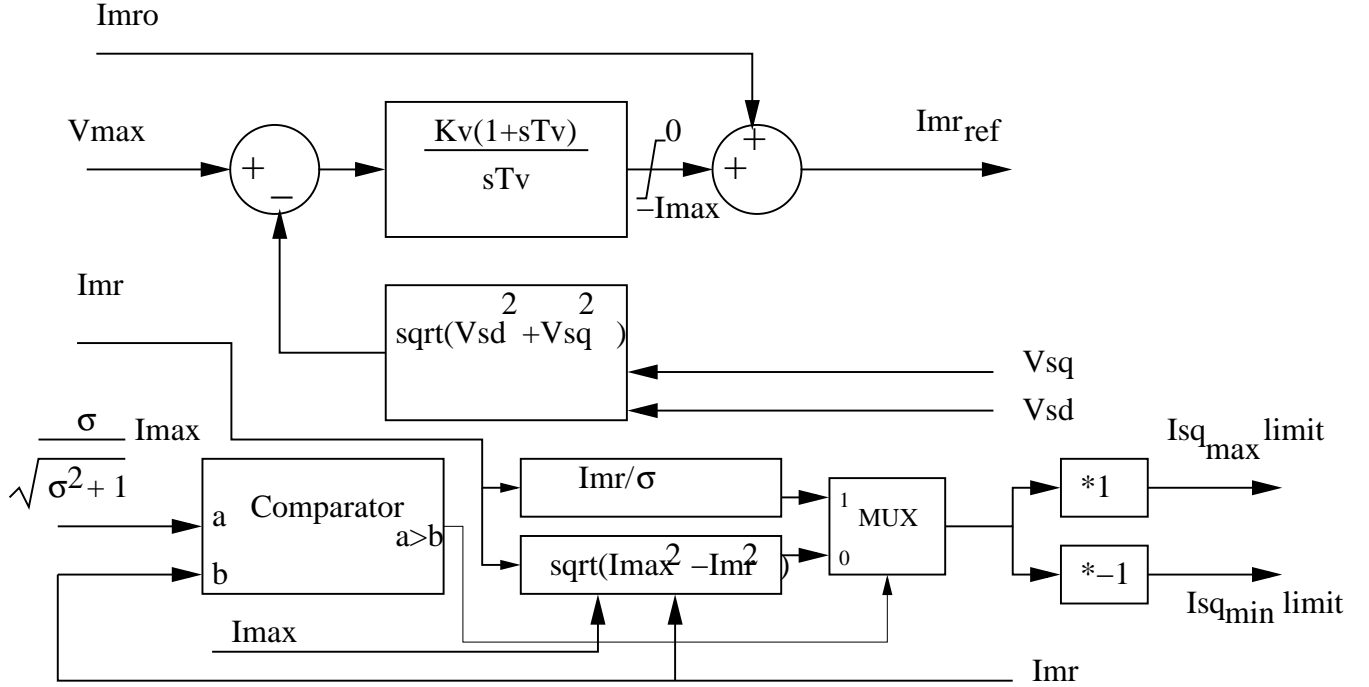


Figure 2.12: Block diagram for field weakening algorithm

When both current and voltage limit are applied and torque(parabola) is to be maximized, it can be proved that maximum torque will occur at the common point. From equation 2.33, 2.35, we get maximum torque when $i_{sd} = \sigma i_{sq}$, which is a line. This can be allowed only when the operating point is inside the current limit circle. Now putting the expression $i_{sd} = \sigma i_{sq}$ in current limit equation, we get

$$i_{sd} = \frac{\sigma}{\sqrt{1+\sigma^2}} i_{max} \quad (2.36)$$

When we are inside the current limit, then $i_{sd} < \frac{\sigma}{\sqrt{1+\sigma^2}} i_{max}$. This can be seen in figure 2.11.

2.4.2 Brief theory of the algorithm

Now based on the points discussed above, one simple algorithm is shown in the figure 2.12. There are two modes of operation in the field weakening region, based on current limit being active or inactive. In the first mode both voltage and current limits are active and the trajectory of the operating points is common points of the circle and ellipse. Because current limit is speed independent, first mode trajectory is the circle's periphery. When ω_1

increases, ellipse radius decreases. After one value of ω_1 ellipse no longer touches the circle, that means maximum torque is achieved when $i_{sd} = \sigma i_{sq}$. This is mode 2. Mode 2 starts when $i_{sd} < \frac{\sigma}{\sqrt{1+\sigma^2}} i_{max}$ is satisfied. As shown in the figure 2.12, one P-I controller is put to keep voltage error zero, whenever voltage limit is violated above base speed. When voltage limit is violated i_{mr} reference is reduced from rated value accordingly. In the mean time i_{sd} is monitored, to decide which mode is active. Here i_{sq} limit is decided by current limit in the first mode and decided by i_{sd} in second mode.

2.4.3 Conclusion

In the above algorithm, we are trying to achieve maximum torque so that overall drive performs very fast. As i_{mr} reference command must not consist any ripple, the voltage controller loop is made very slow to avoid instability. First mode gives higher limit for i_{sq} which is quite expected as current limit is the major limiting factor in this mode. In second mode, voltage limit is major limiting factor, i_{sq} limit keeps decreasing proportionally with i_{sd} to achieve maximum torque on the particular speed.

Chapter 3

Implementation

3.1 Introduction

The algorithms discussed in previous chapter have been implemented together on FPGA (ALTERA)based controller to make a sensorless induction motor drive capable of working in field weakening mode as well as at low speeds. These are prerequisite of field weakening mode operation. Figure 3.1 shows the overall scheme. The present chapter explains the experimental setup and the implementation of the proposed scheme for a 0.37 KW induction motor. Firstly, the details of the experimental setup, which includes Induction motor-DC generator setup, 10 KVA converter, FPGA controller are presented. Then the perunit system followed, and base values for different quantities are defined, which are necessary for the implementation. Later on, all the equations are perunitized and are made ready for implementation.

3.2 Experimental Setup

The experimental setup mainly consists of Induction motor-DC generator setup, 10 KVA inverter, FPGA controller and a PC for programming FPGA. The block diagram in Fig. 3.2 shows the connection among these different entities. The subsequent sections explain the experimental setup in detail[8] and later on implementation is explained.

3.2.1 Induction Motor-DC Generator Setup

As shown in Fig. 3.2, the induction motor terminals are connected to a 10 KVA inverter, which derives power from a DC bus. The DC bus is connected to the output of a 3-phase

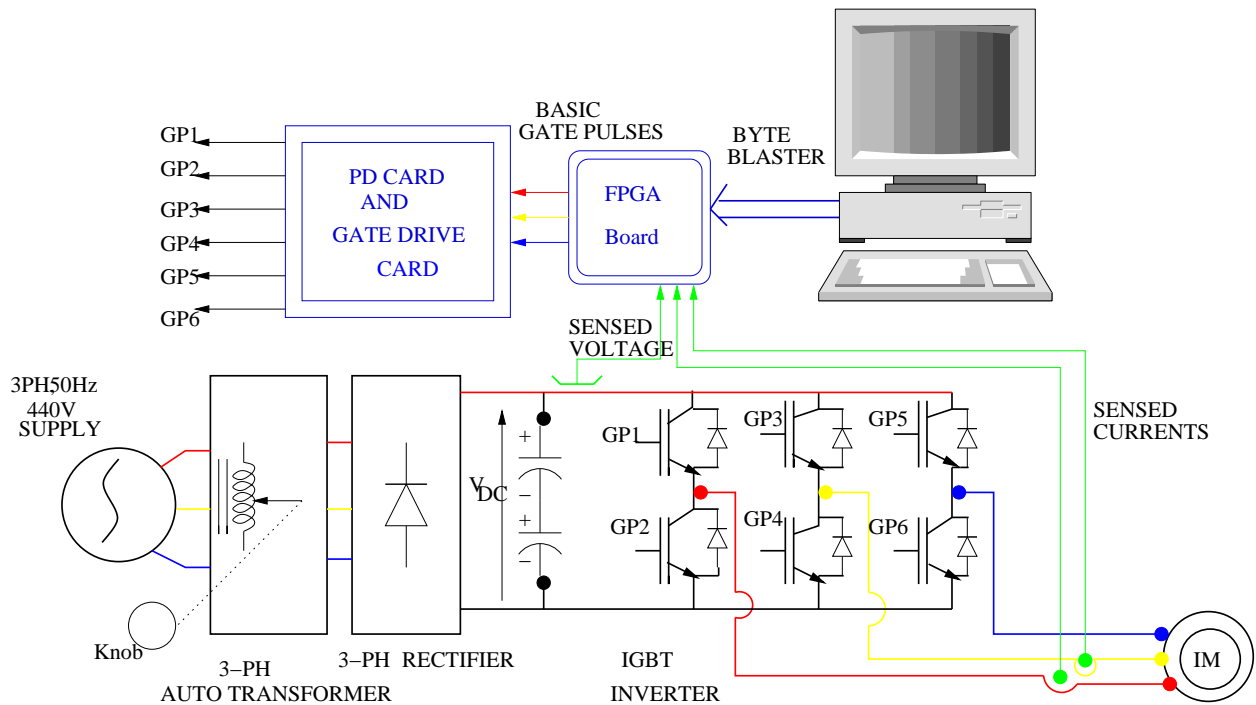


Figure 3.2: Experimental setup

bridge rectifier, fed from a 3-phase auto-transformer. DC bus voltage can be adjusted to a required value by adjusting the auto-transformer. The induction motor is mechanically belt-coupled to a DC generator, whose field is excited from a separate DC source. This DC generator with rheostat connected across its armature terminals forms the loading setup for the induction motor. The details of the induction motor and DC generator are presented in Table. 3.1, Table. 3.3 respectively. The parameters of the Induction motor determined from the no-load test and blocked rotor test are shown in the Table 3.2.

VOLTAGE	220 V
CURRENT	1.98 A
POWER	0.37 KW
POLES	4
SPEED	1500 rpm

Table 3.1: Details of the induction motor

Quantity	Value
R_s	7.1Ω
L_{ls}	$22.6mH$
R_r	7.0Ω
L_{lr}	$22.6mH$
L_0	$283.2mH$

Table 3.2: Parameters of the induction motor

VOLTAGE	30 V
CURRENT	1.5 A
POWER	45 W
SPEED	2000 rpm

Table 3.3: Details of the DC generator

3.2.2 Inverter Setup

The power circuit diagram of the inverter is shown in Fig. 3.2. The power devices used in the inverter are IGBTs. There are three legs in the inverter with two IGBTs (one module) in each leg. The IGBTs are mounted on heat sink and are connected to the DC bus voltage via DC-bus bar. The basic constituents of the inverter apart from the power circuit shown in Fig. 3.2 are PD card, Gate drive card, front panel card, voltage sensing card and current sensing card. The function of each of the circuit is briefly explained in the following subsections.

1. PD Card

The PD (Protection and Delay) card receives three PWM signals from FPGA board via interface card. The circuit on the card generates the complimentary signals with a dead time of $5\ \mu sec$. These six PWM pulses are given as inputs to the gate drive cards. Apart from the delay circuit mentioned above, there is a protection circuit which allows the inverter to trip under faulty conditions such as overcurrent, over-voltage, fault on IGBT.

2. Gate drive Card

A PWM signal received from the PD card is electrically isolated and given as input to the gate of an IGBT with the help of gate drive card. The circuit on the card takes care of the gate current requirement. One gate drive card has two gate drive circuits and hence is used to switch two complimentary IGBT's (i.e., one module) in a leg. Therefore a total of three cards are mounted in the inverter for switching six IGBTs. The circuit gives a low status signal to PD card in case of fault in IGBT for tripping the inverter.

3. Front Panel Card

This card receives the signals from the PD card. The circuit on the card is designed in such a way that the corresponding LEDs glow in case of faults on IGBTs, overvoltage and overcurrent.

4. Voltage Sensing Card

This circuit basically serves the purpose of sensing the DC bus voltage. The output of this card is routed to PD card so that it can trip the inverter and send a signal to the indicator card in case of over voltage in DC-bus. This output is also used for tripping the contactor used in the DC bus charging circuit after the DC-bus voltage reaches the set value.

5. Current Sensing Card

The line currents drawn by the induction motor are sensed by Hall current sensors mounted on this card. The output of this card is 3.348 V/A. This output is fed to ADC on FPGA board via the interface card. This information is further processed in the FPGA, for the implementation of the proposed scheme.

3.2.3 FPGA Controller

The digital platform consists of FPGA device and other devices interfaced to FPGA as shown in Fig. 3.3 [8]. The devices interfaced include configuration device (EEPROM), ADC and DAC; dedicated I/O pins are also provided. The FPGA has logic elements arranged in rows and columns. Each logic element has certain hardware resources which will be utilized to realize the user logic. The vertical and horizontal interconnects of varying speeds provide signal interconnects to implement the custom logic. The choice of an FPGA device for a

given application is based on the size required (number of logic elements), clock speed and number of I/O pins. ALTERA EP1C12Q240C8 is found to be suitable for the given platform. The resources available in this device are listed in Table. 3.4

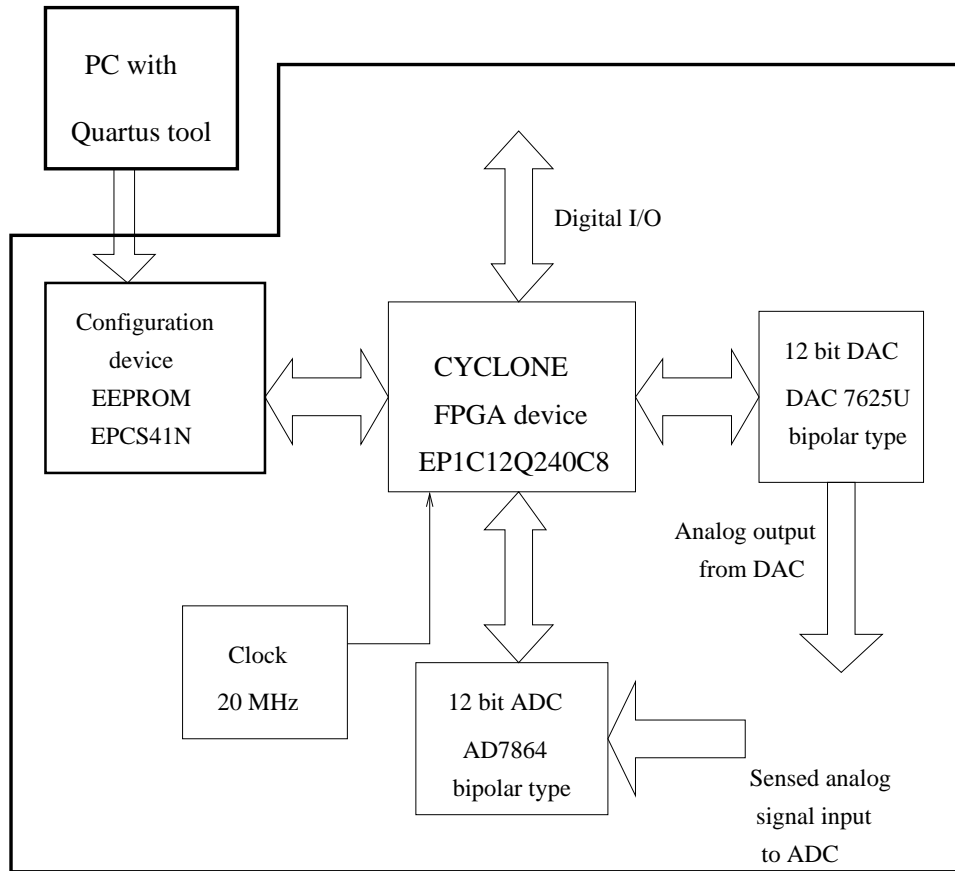


Figure 3.3: Block diagram of FPGA board

1. Configuration Device

The configuration device is an EEPROM (EPCS41N) which is connected to a PC through a parallel port or USB port using ByteblasterII or USB blaster cable. The digital design for the implementation of the proposed scheme is done using Quartus-II (Altera's design tool for FPGA) and the output file after compilation is downloaded to EEPROM through Byteblaster-II or USB blaster cable. The arrangement for configuring the FPGA is shown in Fig. 3.4.

2. On-board Clock

In an FPGA, different blocks of logic elements can operate at different clock frequencies.

Part No	EP1C12Q240C8
Manufacturer	Altera
No of pins	240
No of I/O pins	173
Total internal memory bits	2,39,616
Package	PQFP
No of logic elements	12,060
No of PLL	2
Maximum clock frequency using PLL	275 MHz

Table 3.4: ALTERA FPGA device data

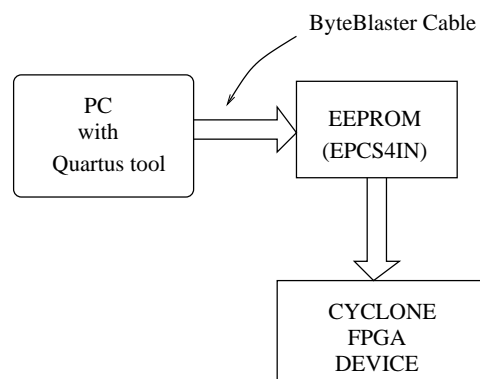


Figure 3.4: Configuration of FPGA device

The board consists of two crystal oscillators both of 20 MHz frequency as shown in Fig. 3.5. Even though two crystal clocks are provided on the board, only one clock is used in the implementation.



Figure 3.5: Block diagram of on-board clock network

3. Digital to Analog Converter

DAC on the board, DAC-7625U, is used to output the digital variables in the controller in analog form. The DAC is a TTL device working with +5V and -5V power supply. This SOIC packaged 12-bit, 28-pin DAC of TEXAS has 4 channels with conversion time of $10\mu\text{sec}$.

4. Analog to Digital Converter

ADC on the board, AD7864AS-1 of Analog devices, is used to convert the analog input signals from the system to digital signals, which are used for further processing. This MQFP packaged, 12-bit, 44-pin simultaneous ADC has 4 channels with a conversion time of $1.6\ \mu\text{sec}$ per channel. There are two such ADCs on the board and hence the board can take 8-analog inputs. It is operated from a +5V power supply but it is bipolar adc.

5. Digital I/Os

Dedicated digital I/Os are necessary to interface to ADC, DAC etc which are present on the board. Apart from that 56 I/O pins are provided for the user to interface application specific hardware.

6. Power Supply Requirements

The cyclone FPGA device requires 1.5V (VCCINT) for its core and I/O voltage (VCCIO) can vary from 1.5V to 3.3V. In this board 3.3V is chosen as I/O voltage for FPGA because most of the interfacing devices on board operated at 3.3V level or above. ADC requires single +5V for its operation. DAC requires +5V, -5V, 2.5V, -2.5V for its op-

eration. On the basis of these requirements 5V and -5V is given as power supply to the board and other levels needed are derived on the board.

3.3 Implementation

The implementation can be divided into two major parts viz.,

- (a) Estimation and calculation of different quantities and
- (b) Controller design and realization.

These are explained in the following sections.

3.4 Estimation and calculation of different quantities

Implementation of the algorithms has been done in 16-bit, 2's complement representation on the FPGA platform. But ADC and DAC are 12-bit, so 4 LSB bits are added as zero and then properly scaled. 1FFF has been chosen as 1 pu, so we have used 16-bit to 16-bit, 32-bit output multipliers and then output is shifted 3-bits left and 16 MSB bits are taken as result. As FPGA chosen has 12K LUTs(Logic units) and a multiplier and a divider cover approximately 3 and 7 percent LUTs respectively. Multiplexing of signals has been done and per algorithm block, one multiplier has been used. FPGA clock is 20 MHz, so all calculation and sampling time will be in 2's multiple of 50 ns. This table shows digital equivalent of its corresponding pu value.

pu value	Equivalent digital Value	Equivalent decimal value
4 pu	$7FFF_H$	32767_d
2 pu	$3FFF_H$	16383_d
1 pu	$1FFF_H$	8191_d
0 pu	0000_H	0_d
-1 pu	$E000_H$	57344_d
-2 pu	$C000_H$	49152_d
-4 pu	8000_H	32768_d

Table 3.5: PU values

3.4.1 Base Values for Different Quantities

As the implementation is digitally realized, there arises the need for following a pu system for simple understanding. For perunitization of different quantities, the base values are required, which can be chosen as per convenience. The Table. 3.6 shows the base values for voltage (chosen as per phase peak of the rated voltage of IM), current (chosen as peak of the rated line current of IM) and frequency (chosen as rated frequency of IM). The other bases are calculated from the above mentioned base quantities. Relation between base quantities are given as,

$$\begin{aligned}
 V_b &= R_b I_b = \omega_b \psi_b = \omega_b L_b I_b \\
 \psi_b &= \frac{V_b}{\omega_b} = L_b I_b \\
 P_b &= \frac{3}{2} V_b I_b \\
 m_b &= \frac{P_b}{\frac{2\omega_b}{P}}
 \end{aligned}$$

Voltage (V_b)	$150 * \frac{\sqrt{2}}{\sqrt{3}} = 122.47V$
Current (I_b)	$1.98 * \sqrt{2} = 2.8A$
Frequency (f_b)	$50Hz$
Frequency in rad/sec (ω_b)	$2\pi * f_b = 314.16rad/sec$
Resistance(R_b)	$\frac{V_b}{I_b} = 43.74\Omega$
Flux linkages(ψ_b)	$\frac{V_b}{\omega_b} = 0.3898 \text{ wb - turns}$
Inductance(L_b)	$\frac{\psi_b}{I_b} = 0.1392 \text{ H}$

Table 3.6: Base values

3.4.2 DC Bus Voltage Calculation

Maximum line to line rms voltage(six step mode) will be 150 V. So we have,

$$\begin{aligned}
 V_{DC} &= 2\frac{\pi}{4}\sqrt{\frac{2}{3}}150V \\
 V_{DC} &= 192.38V
 \end{aligned} \tag{3.1}$$

3.4.3 Sensed Voltage scaling

Rated DC bus voltage 192.38 V produces 5.25 V at the input of ADC(12 bit). It has to give 0.7854 pu as $\frac{V_{DC}}{2}$ (16 bit). So we have to add 4 LSB as zero and then multiply with 3066_d .

3.4.4 Sensed current scaling

One pu current $1.98\sqrt{2}A$ produces 9.3748 V at the input of ADC(12 bit). It has to give 1 pu as I_b (16 bit). So we have to add 4 LSB as zero and then multiply with 2188_d .

3.4.5 Harmonic current extraction

Recalling equations,

$$v_h = R_h i_h + L_h \frac{di_h}{dt} \quad (3.2)$$

Here $L_h = \sigma L_s$ and $R_h = [R_s + R_r (\frac{L_0}{L_r})^2]$.

$$\frac{di_h}{dt} = \frac{1}{L_h} [v_h - R_h i_h]$$

Deviding by $I_b = \frac{V_b}{\omega_b L_b}$ to both sides of the equations, we get

$$\frac{di_{h(pu)}}{dt} = \frac{\omega_b}{L_{h(pu)}} [v_{h(pu)} - R_{h(pu)} i_{h(pu)}]$$

$$\frac{i_h(n+1) - i_h(n)}{Ts} = \frac{\omega_b}{L_{h(pu)}} [v_h(n) - R_{h(pu)} i_h(n)]$$

or

$$i_h(n+1) = i_h(n) + Ts \frac{\omega_b}{L_{h(pu)}} [v_h(n) - R_{h(pu)} i_h(n)] \quad (3.3)$$

Calculation time Ts has been selected as $1.6\mu sec$ on the basis of trial on experimental set up. So we get final equation as

$$i_h(n+1) = i_h(n) + 0.00161_{pu} [v_h(n) - R_{h(pu)} i_h(n)] \quad (3.4)$$

3.4.6 Estimation of speed and position

In the proposed control scheme, basically the quantities that need to be estimated are $\cos\rho$, $\sin\rho$ and speed. From the information of $\cos\rho$ and $\sin\rho$, the speed of the rotor flux $\frac{d\rho}{dt}$ is calculated. i_{sd}, i_{sq}, i_{mr} are also calculated from the information of $i_{s1}, i_{s2}, \cos\rho, \sin\rho$. Slip

frequency can be calculated as $\frac{i_{sq}}{T_r i_{mr}}$. Thus the rotor electrical speed is found by subtracting slip frequency from stator frequency $\frac{d\rho}{dt}$. All the equations necessary for the above calculations are presented in Chapters 2 and 3. These equations are perunitized and are presented here.

$$i_{sa(pu)} = \frac{3}{2} i_{s1(pu)}$$

This equation in digital domain can be written as,

$$i_{sa}(n) = 1.5_{pu} i_{s1}(n) \quad (3.5)$$

$$i_{sb(pu)} = \frac{\sqrt{3}}{2} (i_{s2(pu)} - i_{s3(pu)})$$

$$i_{sb}(n) = 0.866_{pu} (i_{s2}(n) - i_{s3}(n)) \quad (3.6)$$

$$e_{sa(pu)} = v_{sa(pu)} - i_{sa(pu)} R_{s(pu)}$$

$$e_{sa}(n) = v_{sa}(n) - 0.1623_{pu} i_{sa}(n) \quad (3.7)$$

$$e_{sb(pu)} = v_{sb(pu)} - i_{sb(pu)} R_{s(pu)}$$

$$e_{sb}(n) = v_{sb}(n) - 0.1623_{pu} i_{sb}(n) \quad (3.8)$$

Recalling the equation for determining the flux linkages,

$$\underline{\psi}_s^s = \int [(\underline{v}_s^s - R_s \underline{i}_s^s) + K(\underline{\psi}_r^{s*} - \underline{\psi}_r^s)] dt$$

In time domain, above equation can be written as,

$$\frac{d\psi_{sa}}{dt} = V_{terms}$$

Dividing the above equation by V_b ,

$$\frac{1}{\omega_b} \frac{d\psi_{sa(pu)}}{dt} = V_{terms}(pu)$$

$$\psi_{sa}(n+1) = \psi_{sa}(n) + V_{terms}(n) \omega_b T_s$$

Choosing the value of $T_s = 12.8 \mu sec$

$$\psi_{sa}(n+1) = \psi_{sa}(n) + \frac{33}{8191} V_{terms}(n) \quad (3.9)$$

Similarly, the equation for $\psi_{sb}(n)$ is obtained, Recalling the equation for rotor flux linkages,

$$\psi_{ra}^s = \frac{L_r}{L_0} [\psi_{sa} - \sigma L_s i_{sa}]$$

This is same in per unit as well. The equations for $\cos\rho, \sin\rho$ in pu can be written as follows,

$$\cos\rho(n) = \frac{\psi_{ra}^s(n)}{|\underline{\psi}_r^s(n)|} \quad (3.10)$$

Similarly,

$$\sin\rho(n) = \frac{\psi_{rb}^s(n)}{|\underline{\psi}_r^s(n)|} \quad (3.11)$$

Recalling the equation for rotor flux speed, ω ,

$$\omega 1 = \frac{d\rho}{dt} = \cos\rho \frac{d}{dt}(\sin\rho) - \sin\rho \frac{d}{dt}(\cos\rho)$$

Dividing the equation with ω_b ,

$$\omega 1 (pu) = \frac{1}{\omega_b} \left(\cos\rho \frac{d}{dt}(\sin\rho) - \sin\rho \frac{d}{dt}(\cos\rho) \right)$$

$$\begin{aligned} \omega 1(n) &= \frac{1}{\omega_b T_s} [\cos\rho(n) (\sin\rho(n+1) - \sin\rho(n)) - \sin\rho(n) (\cos\rho(n+1) - \cos\rho(n))] \\ \omega 1(n) &= 7.77_{pu} [\cos\rho(n) \sin\rho(n+1) - \sin\rho(n) \cos\rho(n+1)] \end{aligned} \quad (3.12)$$

$$i_{sd}(n) = i_{sa}(n) \cos\rho(n) + i_{sb}(n) \sin\rho(n) \quad (3.13)$$

$$i_{sq}(n) = i_{sb}(n) \cos\rho(n) - i_{sa}(n) \sin\rho(n) \quad (3.14)$$

The equation for i_{mr} in frequency domain is,

$$i_{mr} = \frac{1}{1 + sT_r} i_{sd}$$

In time domain it can be written as

$$i_{mr} = \frac{1}{T_r} \int (i_{sd} - i_{mr}) dt$$

Dividing the equation with I_b ,

$$i_{mr(pu)} = \frac{1}{T_r} \int (i_{sd(pu)} - i_{mr(pu)}) dt$$

$$i_{mr}(n+1) = i_{mr}(n) + \frac{T_s}{T_r} [i_{sd}(n) - i_{mr}(n)]$$

Here sampling time $T_s = 204.8 \mu sec$, so we get,

$$i_{mr}(n+1) = i_{mr}(n) + \frac{38}{8191} [i_{sd}(n) - i_{mr}(n)] \quad (3.15)$$

Recalling the equation for slip frequency, ω_{slip} ,

$$\omega_{slip} = \frac{i_{sq}}{T_r i_{mr}}$$

Dividing with frequency base, ω_b ,

$$\begin{aligned}\omega_{slip(pu)} &= \frac{1}{\omega_b T_r} \left(\frac{i_{sq}}{i_{mr}} \right) \\ \omega_{slip}(n) &= 0.073_{pu} \left(\frac{i_{sq}(n)}{i_{mr}(n)} \right)\end{aligned}\quad (3.16)$$

The machine electrical speed, ω , is given by

$$\omega(n) = \omega_1(n) - \omega_{slip}(n) \quad (3.17)$$

Except these mentioned equations, other equations do not change while perunitization. The digital realization for all equations requires adders, subtractors, multipliers and dividers. All these entities are available in the library of Quartus-II tool. Apart from these arithmetic logic entities, D-Flip Flops are also needed for storing previous data values, in the case of performing integration.

3.4.7 Selection of K in flux position estimator block

As explained earlier, K is selected on trial basis. Here we have picked up a value $K = 0.75_{pu}$, which is suitable to overall model. Value of K is sensitive to controller and machine parameters.

3.4.8 Decoupling Circuit

As discussed in the second chapter, the decoupling terms are,

$$\begin{aligned}v_{sdx} &= -\frac{\sigma L_s \omega_1 i_{sq}(t)}{G} + \frac{(1 - \sigma) L_s \frac{di_{mr}}{dt}}{G} \\ v_{sqx} &= \frac{\sigma L_s \omega_1 i_{sd}(t)}{G} + \frac{(1 - \sigma) L_s \omega_1 i_{mr}(t)}{G}\end{aligned}$$

While perunitizing the above equations, G is considered as 1 pu because it is assumed that for a 1 pu peak modulating wave, the average output pole voltage of the inverter is the rated per phase peak voltage of the induction motor, which is chosen as base value.

$$v_{sdx(pu)} = -\sigma L_{s(pu)} \omega_{1(pu)} i_{sd(pu)} + (1 - \sigma) L_{s(pu)} \frac{1}{\omega_b} \frac{di_{mr}}{dt}$$

or

$$v_{sdx}(pu) = -\sigma L_{s(pu)} \omega_{1(pu)} i_{sd(pu)} + (1 - \sigma) L_{s(pu)} \frac{1}{\omega_b T_r} (i_{sd(pu)} - i_{mr(pu)})$$

$$v_{sqx}(pu) = \sigma L_{s(pu)} \omega_{1(pu)} i_{sq(pu)} + (1 - \sigma) L_{s(pu)} \omega_{1(pu)} i_{mr(pu)}$$

In digital domain these equations can be written as,

$$v_{sdx}(n) = -0.312_{pu} \omega_1(n) i_{sd}(n) + 0.1376_{pu} (i_{sd(pu)} - i_{mr(pu)}) \quad (3.18)$$

$$v_{sqx}(n) = 0.312_{pu} \omega_1(n) i_{sq}(n) + 1.8838_{pu} \omega_1(n) i_{mr}(n) \quad (3.19)$$

3.5 Design and implementation of Controllers

The closed loop control of induction motor in field weakening mode involves following controllers viz., voltage controller, speed controller, flux controller and two current controllers. All the controllers are PI controllers. In this subsection, the controller's design is presented. All signals are supposed to be in per unit, so controller parameters will be inherently in per unit.

3.5.1 General digital implementation of a controller

Let's take x as input(pu) and y as output(pu) of a PI-controller, K and T are it's parameters, T_s is calculation time. We have,

$$y = K \frac{(1 + sT)}{sT} x$$

$$y = Kx + \frac{K}{sT} x$$

Let's take $z = \frac{K}{sT} x$, so $y = Kx + z$.

$$\frac{d}{dt} z = \frac{K}{T} x$$

In discrete terms it will become,

$$\frac{z(n+1) - z(n)}{T_s} = \frac{K}{T} x(n)$$

$$z(n+1) = z(n) + \frac{KT_s}{T} x(n)$$

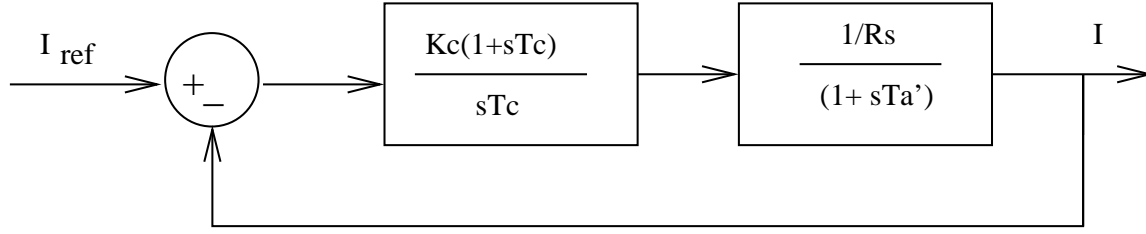


Figure 3.6: Current loop

And finally we have

$$y(n) = Kx(n) + z(n)$$

3.5.2 Design of Current Controller

Speed loop forms the outer loop and current(i_{sq}) loop forms the inner one. Similarly flux loop is the outer loop and current(i_{sd}) loop is the inner loop. Both current loops are similar and these can be drawn as shown in Fig. 3.6. All the controllers are designed for the per unit models shown in the figures here.

The current controller time constant(T_c) is chosen as the system largest time constant in the current loop($T_c = \frac{\sigma L_s}{R_s} = T_a$). Practically (T_c) is chosen on simulation basis to consider the effect of $D - Q$ to $a - b$ and reverse transformations as the sensorless algorithm is used. ($T_c = T_{a'}$) and $T_{a'} = 10 T_a$ The transfer function for the current loop can be written as,

$$\frac{i(s)}{i^*(s)} = \frac{\left(\frac{K_c}{sT_c}\right) \left(\frac{1}{R_s}\right)}{1 + \left(\frac{K_c}{sT_c}\right) \left(\frac{1}{R_s}\right)}$$

Simplifying and approximating the above equation results in the following transfer function.

$$\frac{i(s)}{i^*(s)} = \frac{1}{1 + s \left(\frac{R_s T_c}{K_c}\right)} \quad (3.20)$$

By choosing the bandwidth less than carrier frequency, the expression for the gain can be obtained as,

$$K_c = R_s T_c \omega_{cutoff} \quad (3.21)$$

Here $\omega_{cutoff} = 60 \text{ radian per seconds}$.

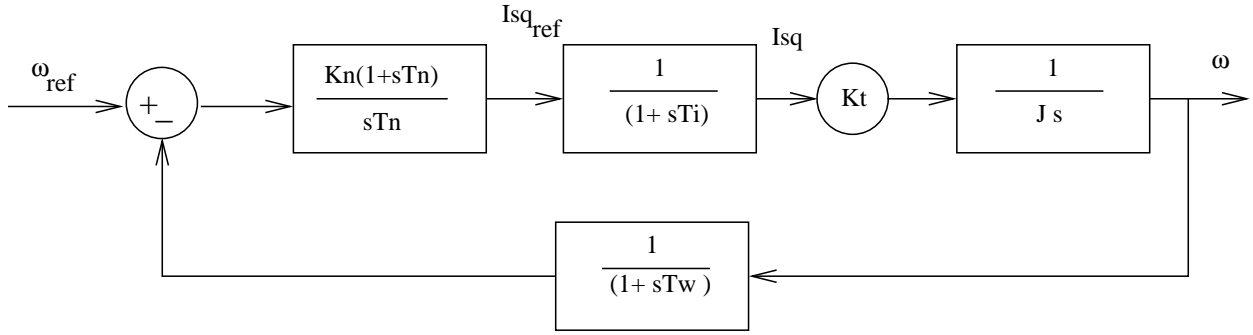


Figure 3.7: Speed loop

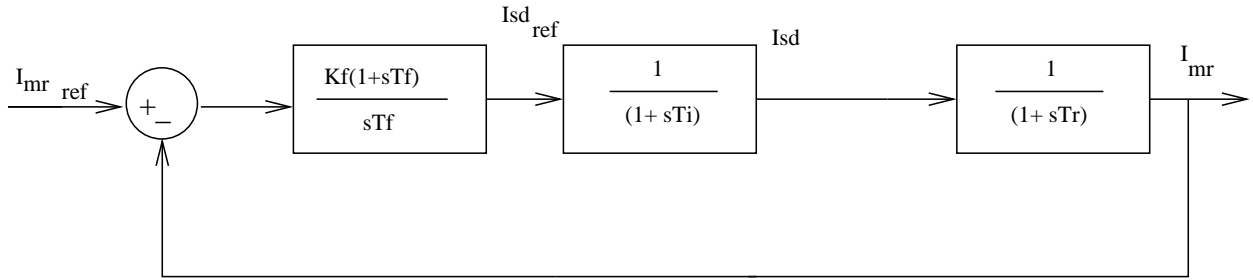


Figure 3.8: Flux loop

3.5.3 Design of Speed Controller

Approximating the current loop transfer function by first order system as $\frac{i(s)}{i^*(s)} = \frac{1}{1+s(T_i)}$, the speed loop can be drawn as shown in Fig. 3.7. Here we use a first order speed filter such that $(T_w = \frac{1}{120} \gg T_i)$ as shown in figure. Now we select a value of $(T_N = 4(2T_i + T_w))$ on the basis of symmetric optimum method [4]. Hence the gain and time constant for the speed controller are obtained as follows,

$$T_N = 4(2T_i + T_w) \quad (3.22)$$

$$K_N = \frac{2J}{K_t T_N} \quad (3.23)$$

Here $K_t = \frac{P}{3}(1 - \sigma)L_s i_{mr}(0)$. And in per unit $K_{t(pu)} = K_t \frac{I_b}{m_b}$.

3.5.4 Design of Flux Controller

The flux loop can be drawn as shown in Fig. 3.8. Choosing the controller time constant as

The controller parameters are tabularized and presented in the Table. 3.7.

Current Controller		Speed Controller		Flux Controller		Voltage Controller	
K_c	T_c	K_N	T_N	K_F	T_F	K_v	T_v
0.596	61.2 msec	9.83	193 msec	1.09	43.6 msec	1.5	100 msec

Table 3.7: Controller parameters

3.6 Conclusion

The chapter presented the details of the experimental setup and the development of equations in perunit system. The design of the controllers and their realization are also discussed. The experimental results in different conditions are presented in the next chapter.

Chapter 4

Experimental Results

4.1 Introduction

The experimental setup is explained in detail in previous chapter. In this chapter, the experimental results are presented under different conditions. The results under steady state operation and transient operation are presented. First DC bus is charged to 192.4 V as calculated in the previous chapter. Then, the program developed for sensorless vector control in Quartus II tool is burnt into FPGA.

4.2 Current Extraction Waveforms

These results show fundamental current extraction. Refer Figs. 4.1, 4.2, 4.3, 4.4, 4.5, 4.6

4.3 Overmodulation Waveforms

These results show overmodulation waveforms. Refer Figs. 4.7, 4.8, 4.9, 4.10

4.4 Steady State Waveforms

Under steady state operation with a load of 400W, the different cases are discussed and the corresponding results for these cases are shown. For each of the cases the following waveforms are recorded:

Unit vectors $\cos\rho$ and $\sin\rho$,

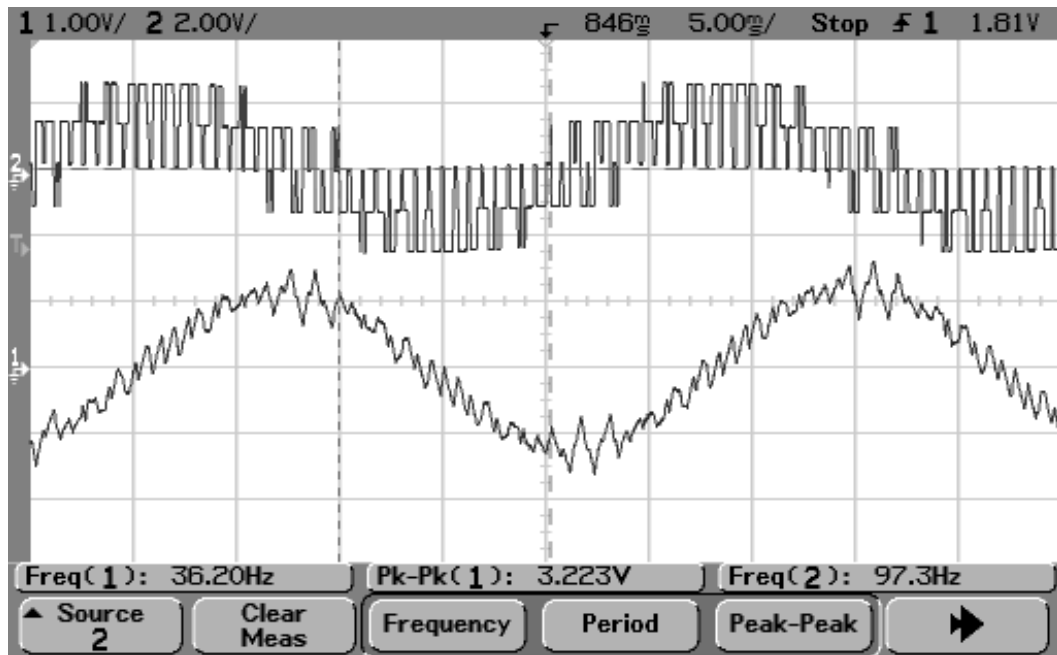


Figure 4.1: V_{rn} and i_{sr} waveforms for speed command of $0.7pu$ ($35Hz$)

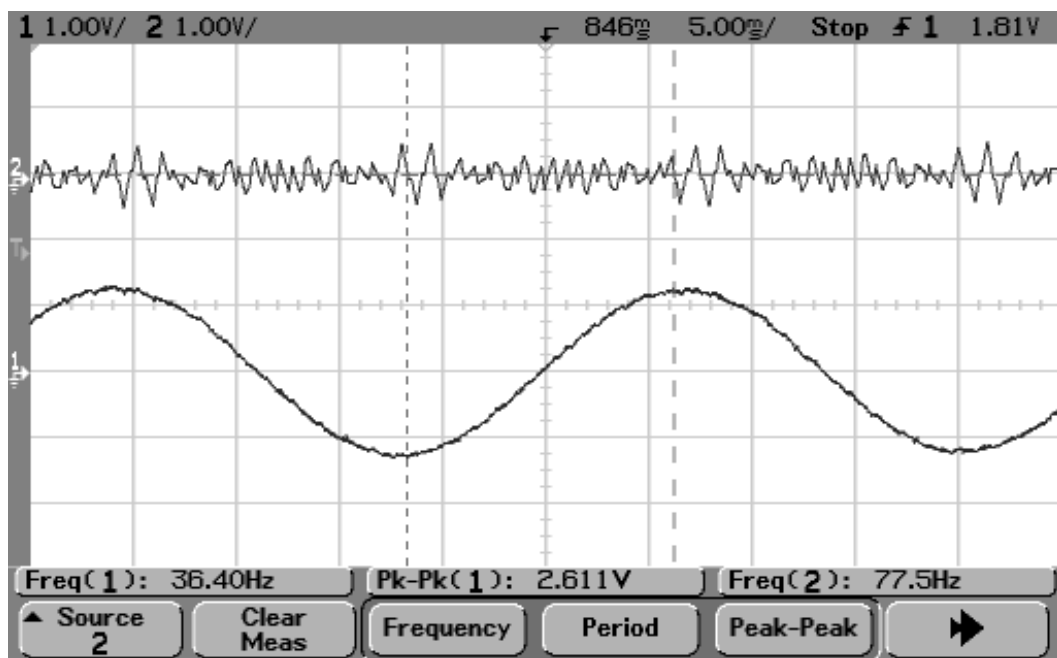


Figure 4.2: i_{rh} and i_{sr} (extracted) waveforms for speed command of $0.7pu$ ($35Hz$)

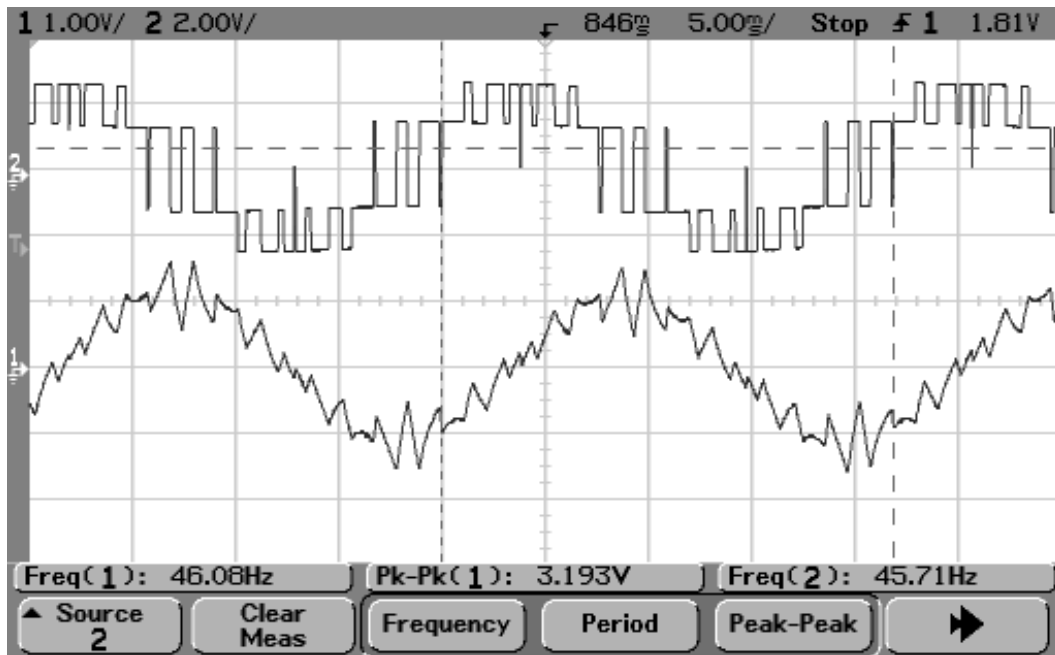


Figure 4.3: V_{rn} and i_{sr} waveforms for speed command of $0.92pu$ ($46Hz$)

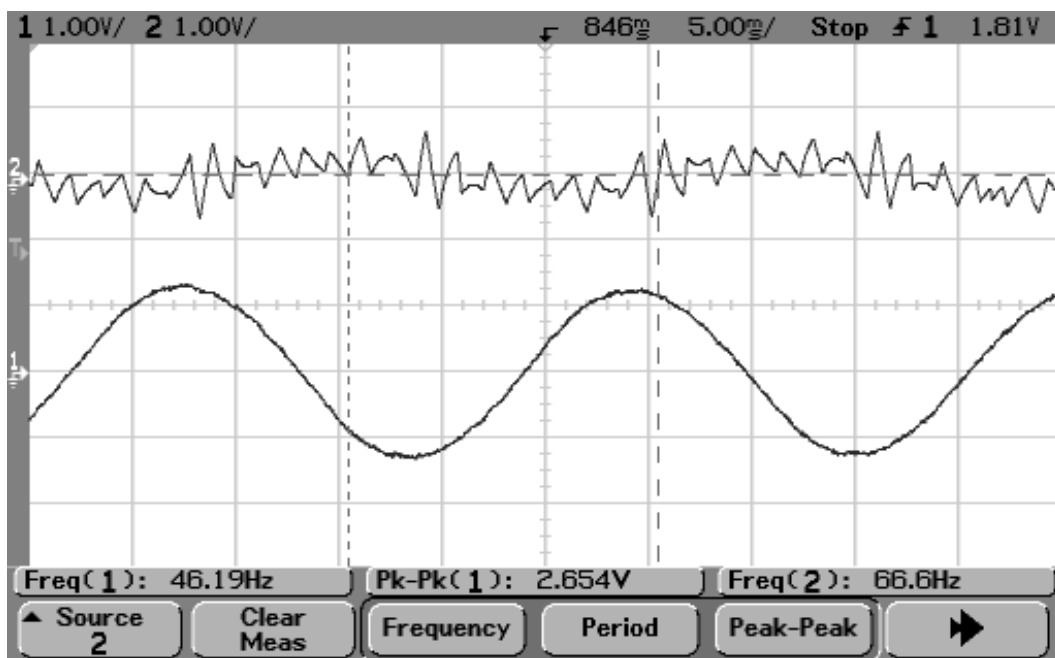


Figure 4.4: i_{rh} and $i_{sr}(extracted)$ waveforms for speed command of $0.92pu$ ($46Hz$)

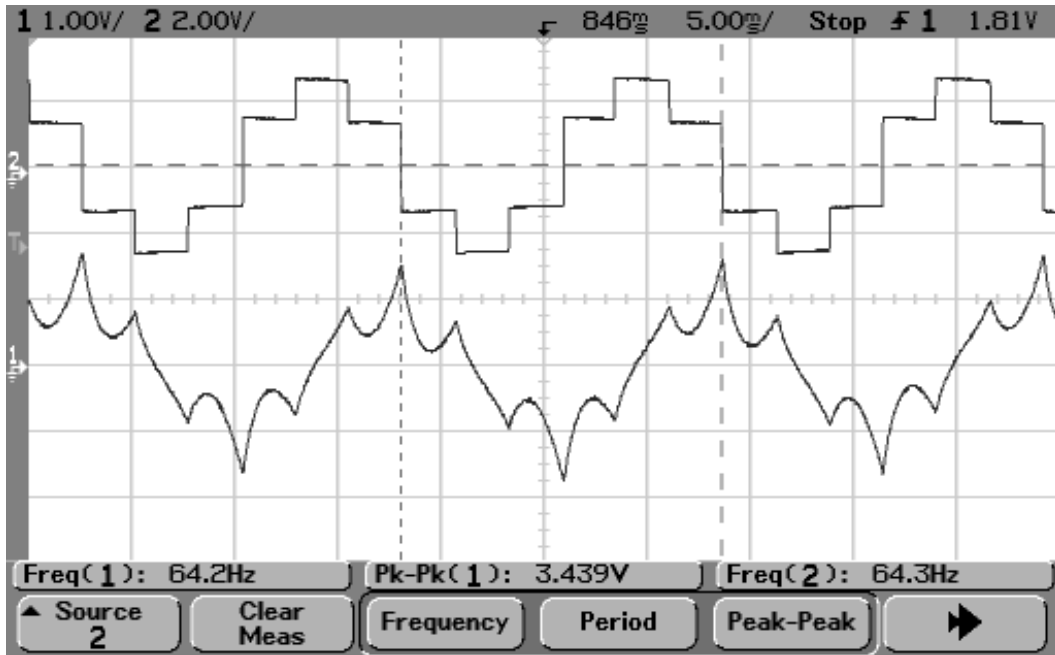


Figure 4.5: V_{rn} and i_{sr} waveforms for speed command of $1.25pu$ ($64Hz$)

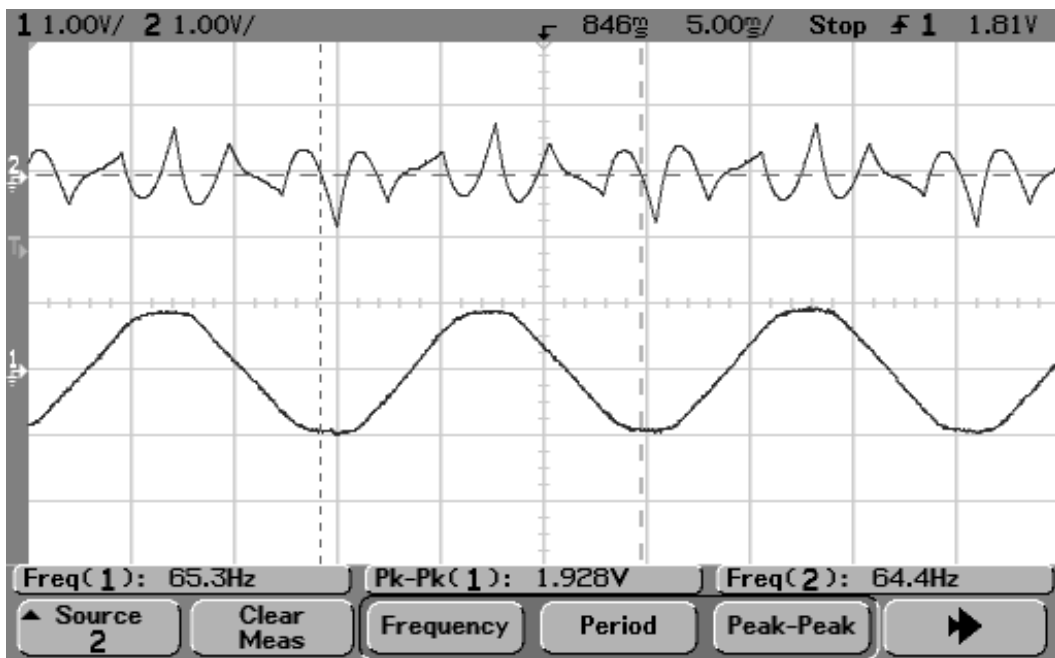


Figure 4.6: i_{rh} and i_{sr} (extracted) waveforms for speed command of $1.25pu$ ($64Hz$)

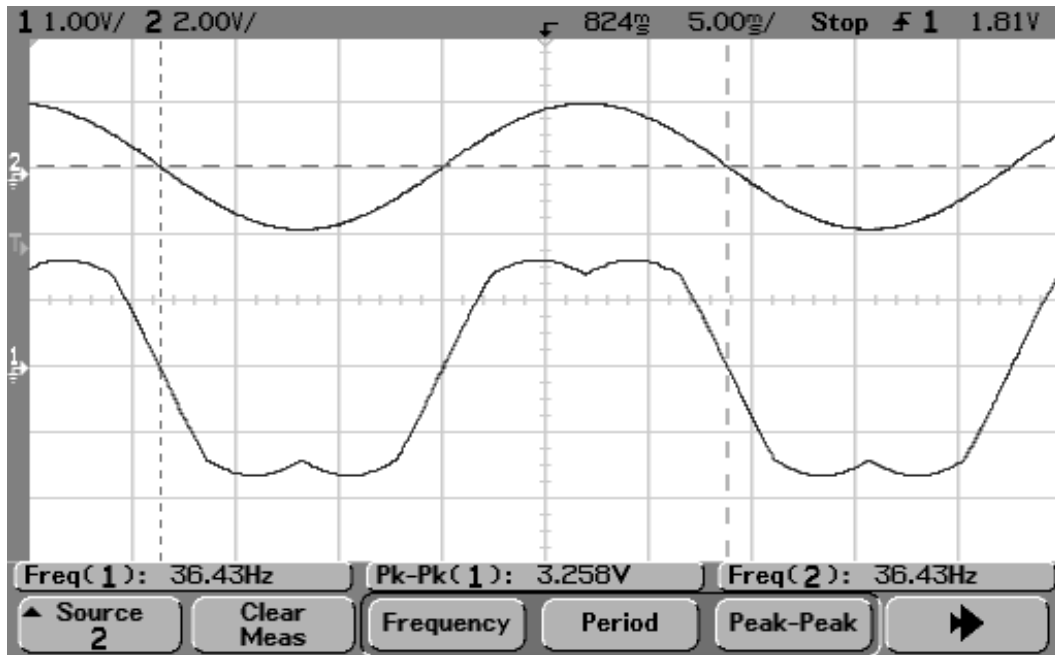


Figure 4.7: V_{ref} and $V_{svpwm(modified)}$ waveforms for speed command of $0.75pu$ ($36Hz$)

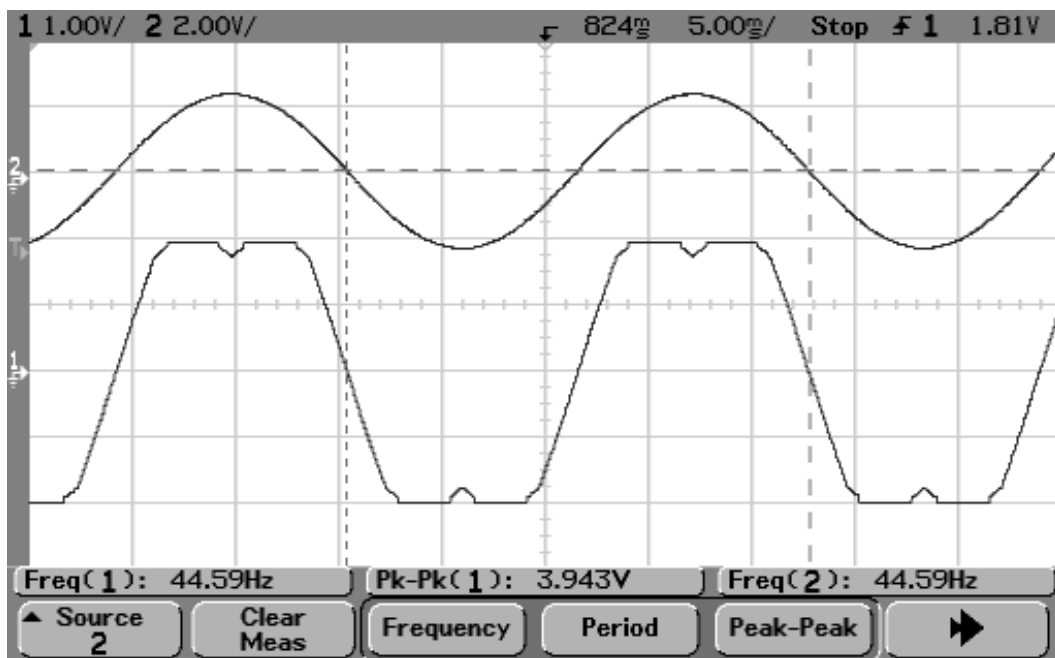


Figure 4.8: V_{ref} and $V_{svpwm(modified)}$ waveforms for speed command of $0.89pu$ ($44.5Hz$)

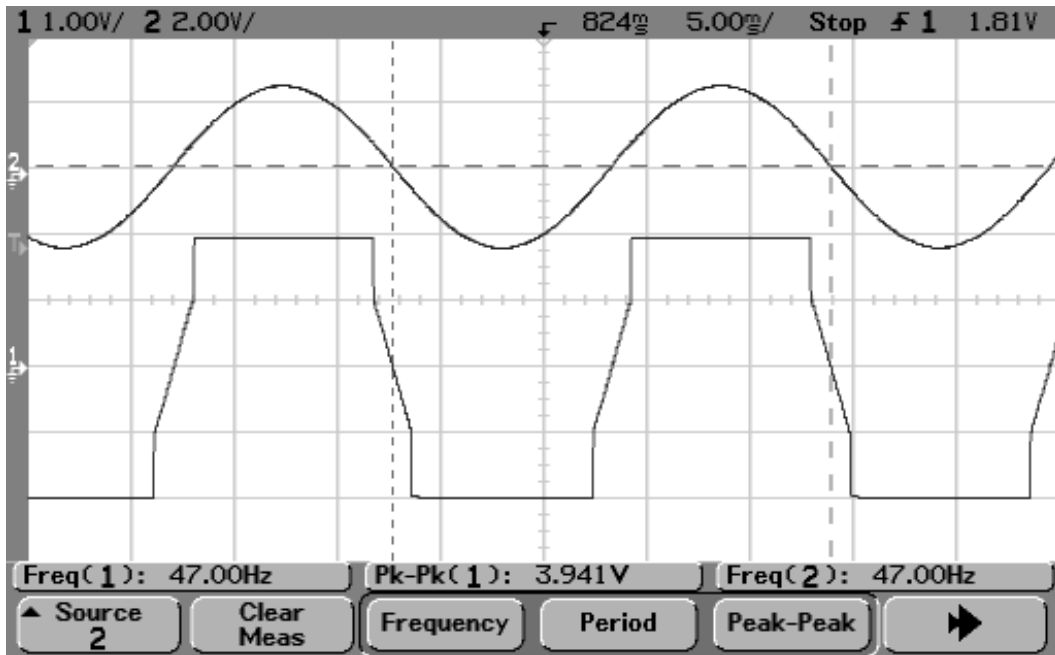


Figure 4.9: V_{ref} and $V_{svpwm(modified)}$ waveforms for speed command of $0.94pu$ ($47Hz$)

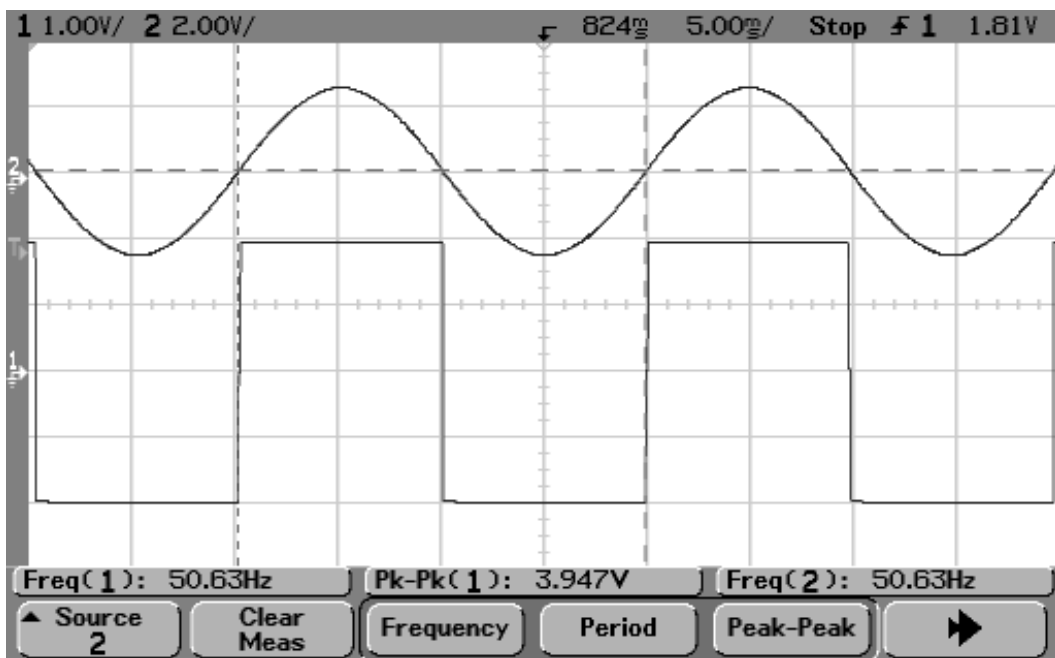


Figure 4.10: V_{ref} and $V_{svpwm(modified)}$ waveforms for speed command of $01.02pu$ ($50.6Hz$)

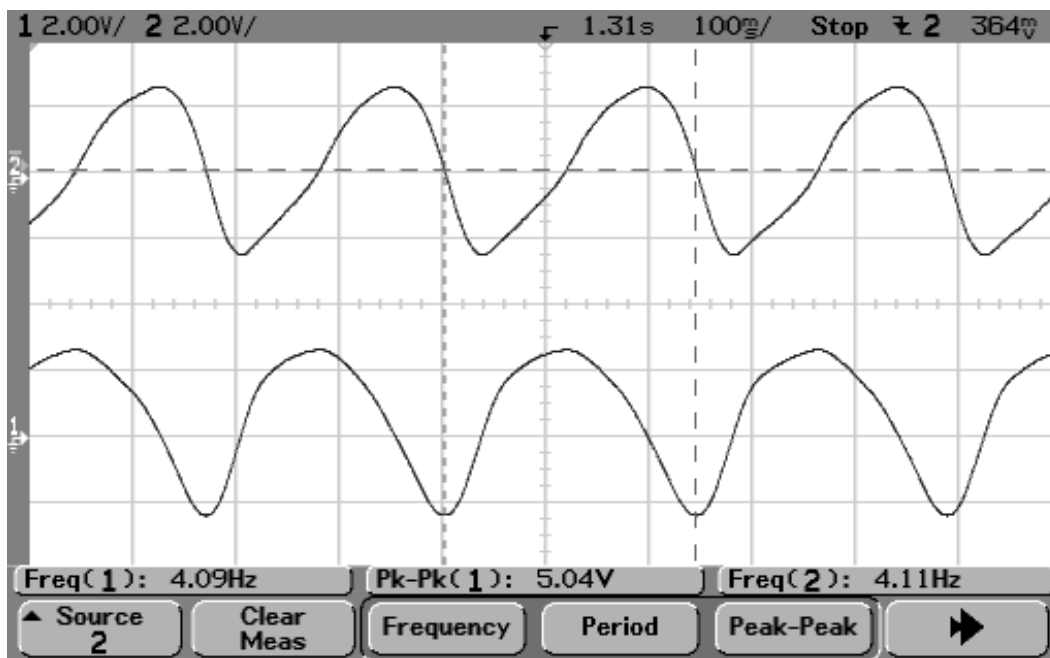


Figure 4.11: $\sin\theta$ and $\cos\theta$ waveforms for speed command of $0.0625 pu$ ($3.125 Hz$)

Line currents i_{s1}, i_{s2} ,

Currents in (d,q) coordinate system i_{sd}, i_{sq} .

Case 1: Speed command of $0.0625 pu$ i.e., $3.125 Hz$

Refer Figs. 4.11, 4.12, 4.13

Case 2: Speed command of $0.75 pu$ i.e., $37.5 Hz$

Refer Figs. 4.14, 4.15, 4.16

Case 3: Speed command of $1.5 pu$ i.e., $75 Hz$

Refer Figs. 4.17, 4.18, 4.19.

Case 4: Speed command of $2.25 pu$ i.e., $112.5 Hz$

Refer Figs. 4.20, 4.21, 4.22

4.5 Transient Waveforms

Under transients section, the different cases are discussed and the corresponding results for these cases are shown. For each of the cases the following waveforms are recorded:

Rotor speed ω ,

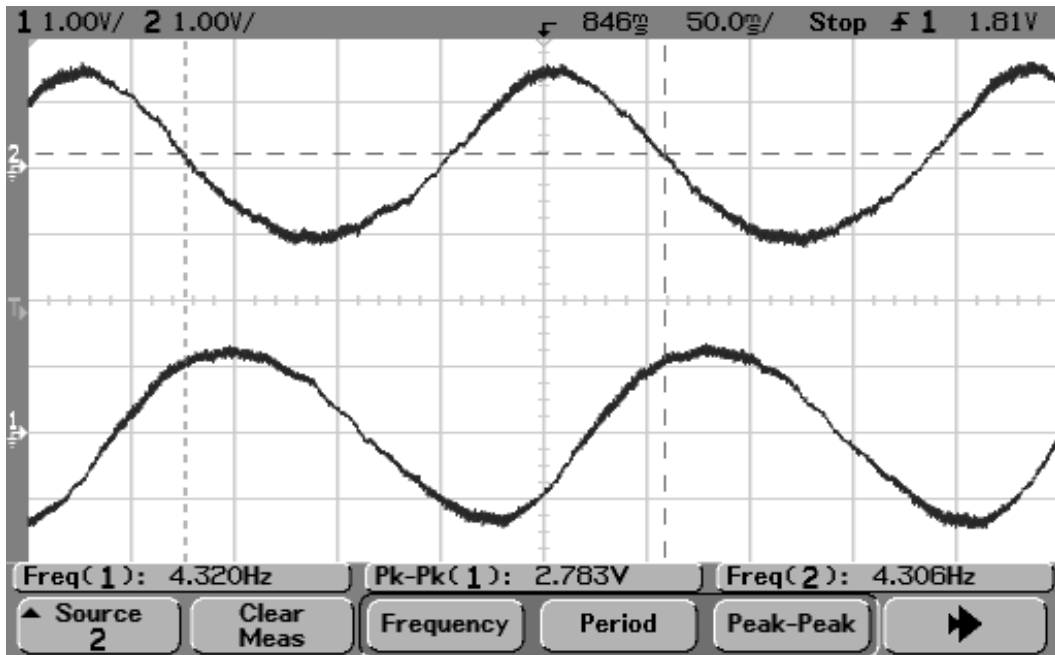


Figure 4.12: i_{s1} and i_{s2} waveforms for speed command of $0.0625pu$ ($3.125Hz$)

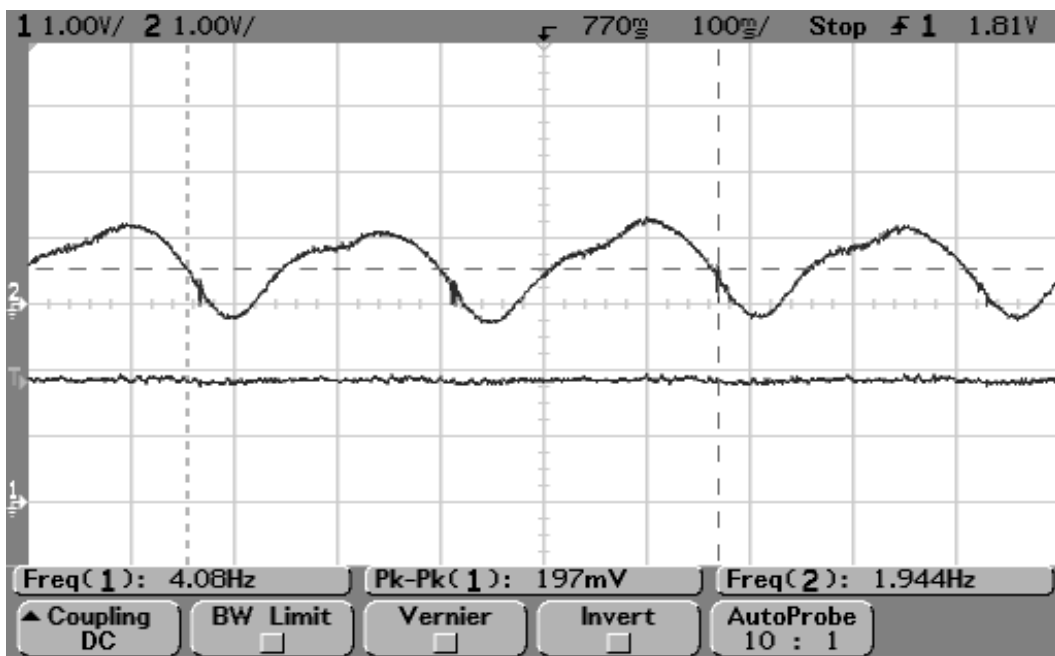


Figure 4.13: i_{sq} and i_{sd} waveforms for speed command of $0.0625pu$ ($3.125Hz$)

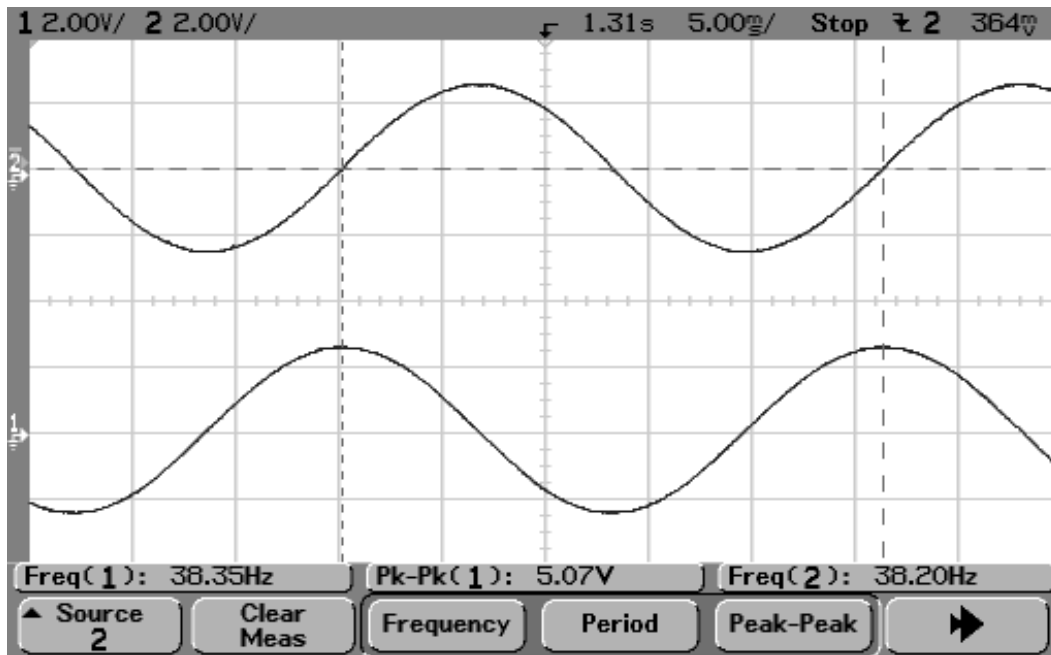


Figure 4.14: $\sin\rho$ and $\cos\rho$ waveforms for speed command of $0.75pu$ ($37.5Hz$)

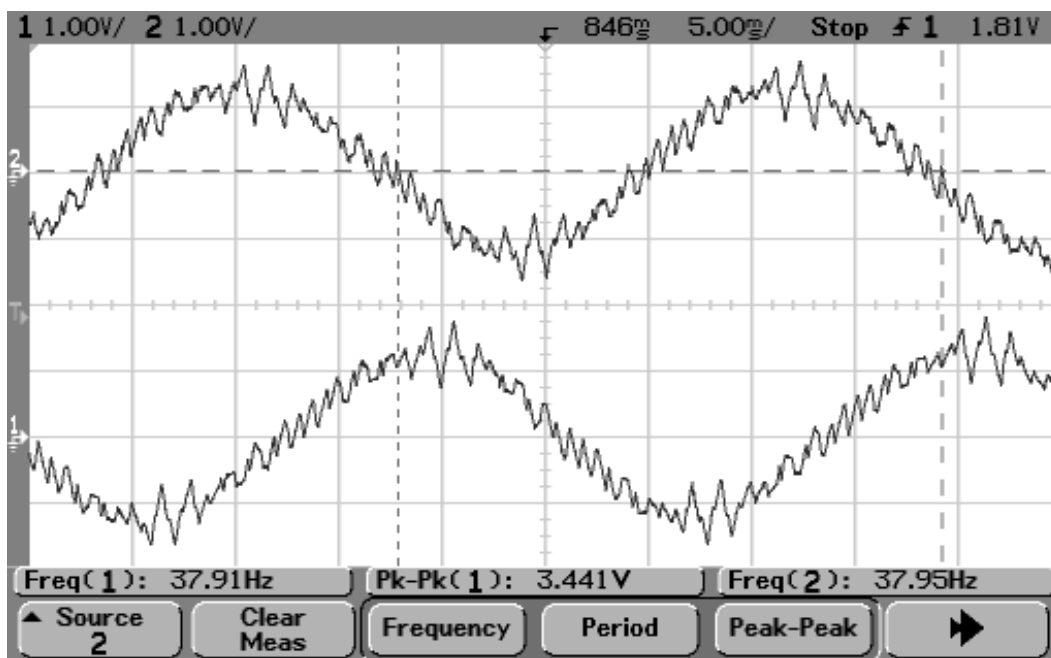


Figure 4.15: i_{s1} and i_{s2} waveforms for speed command of $0.75pu$ ($37.5Hz$)

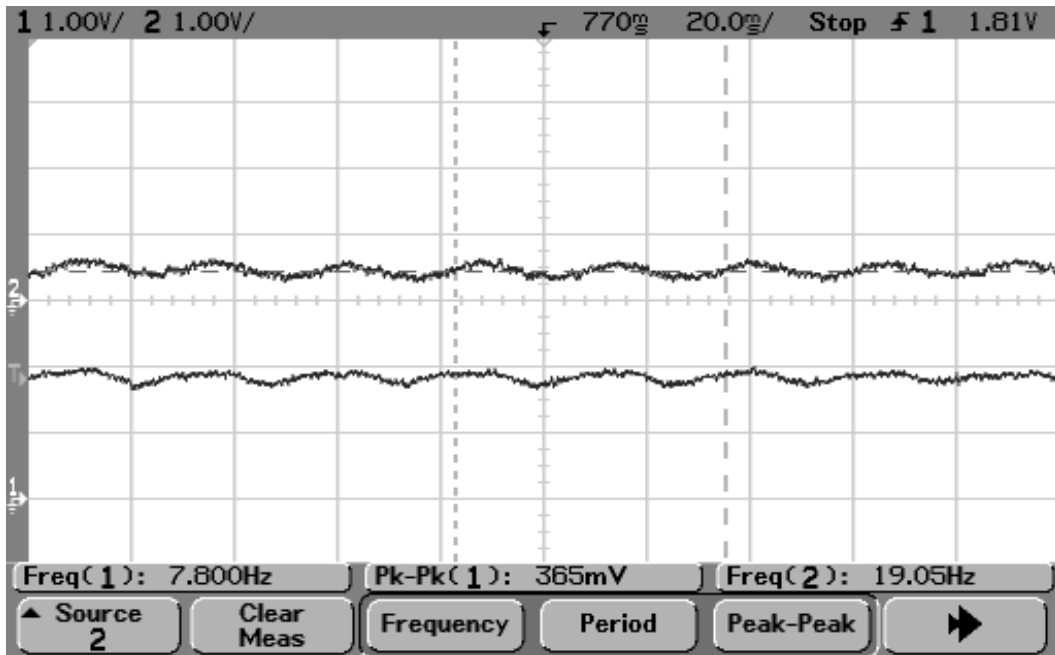


Figure 4.16: i_{sq} and i_{sd} waveforms for speed command of $0.75pu$ ($37.5Hz$)

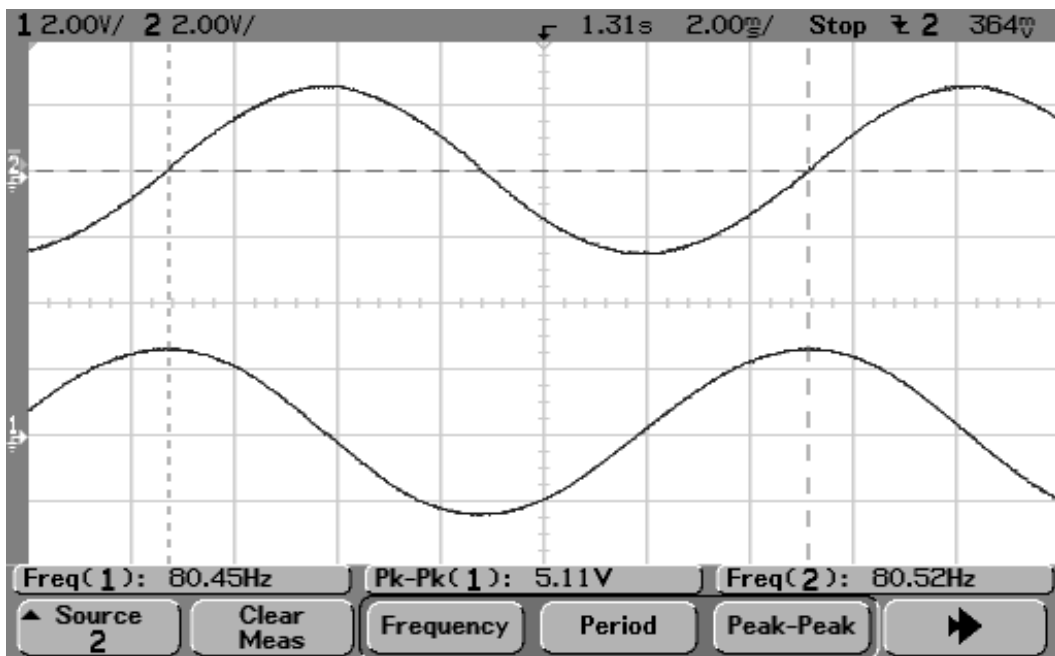


Figure 4.17: $\sin p$ and $\cos p$ waveforms for speed command of $1.5pu$ ($75Hz$)

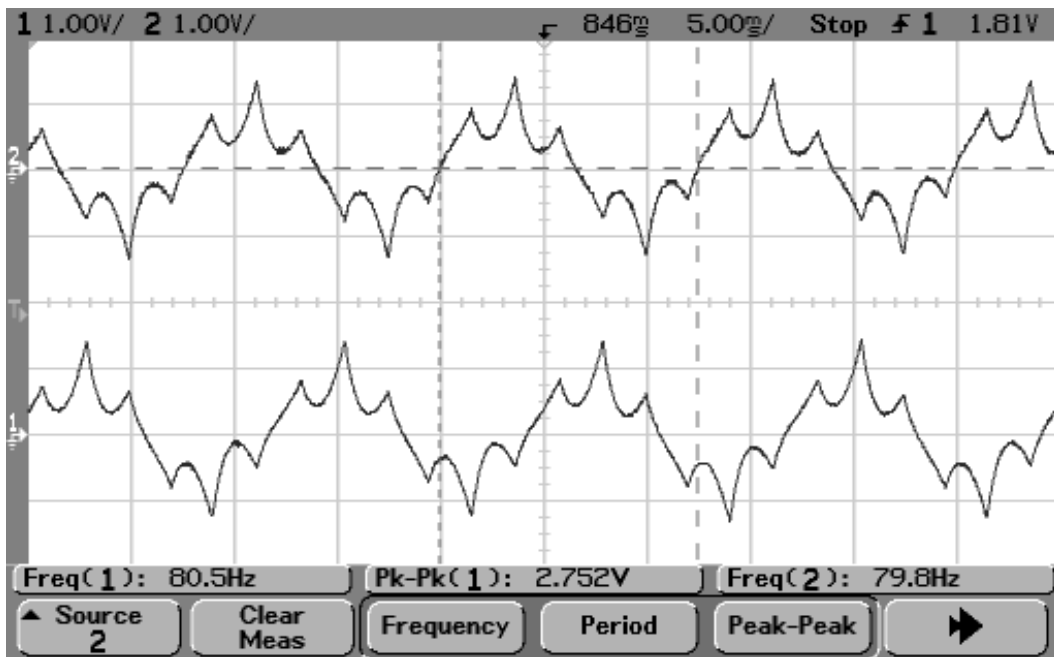


Figure 4.18: i_{s1} and i_{s2} waveforms for speed command of $1.5pu$ ($75Hz$)

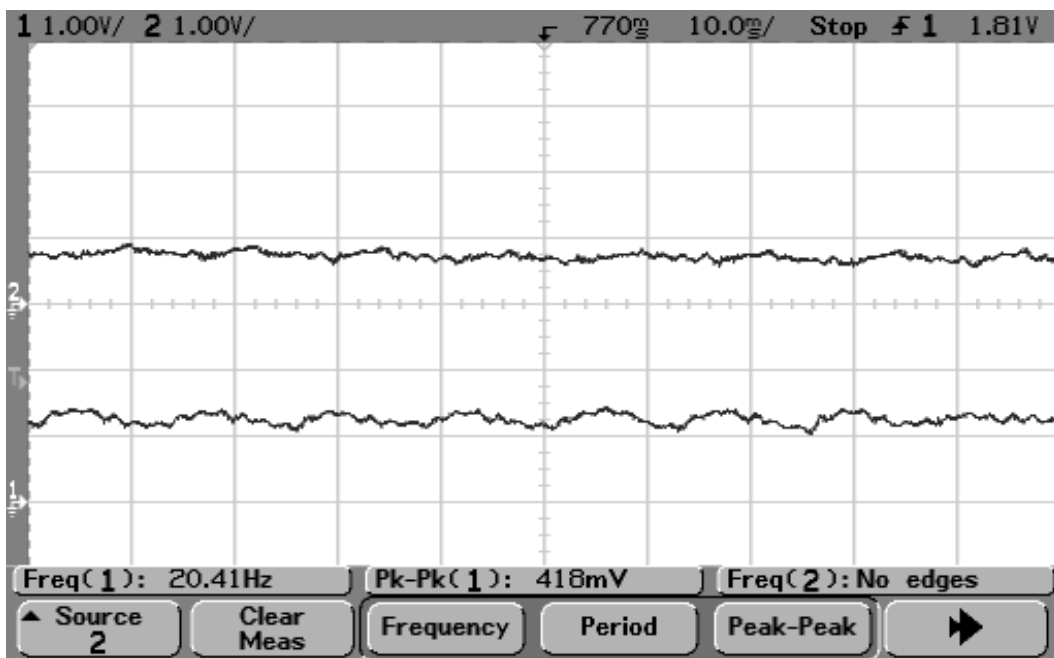


Figure 4.19: i_{sq} and i_{sd} waveforms for speed command of $1.5pu$ ($75Hz$)

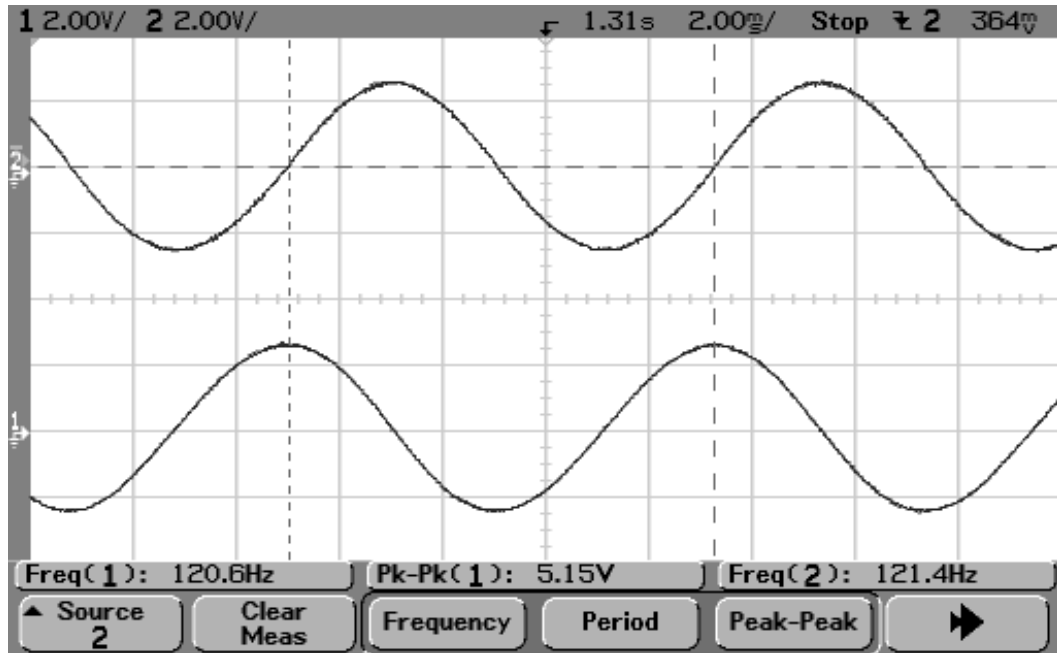


Figure 4.20: $\sin\varphi$ and $\cos\varphi$ waveforms for speed command of $2.25pu$ ($112.5Hz$)

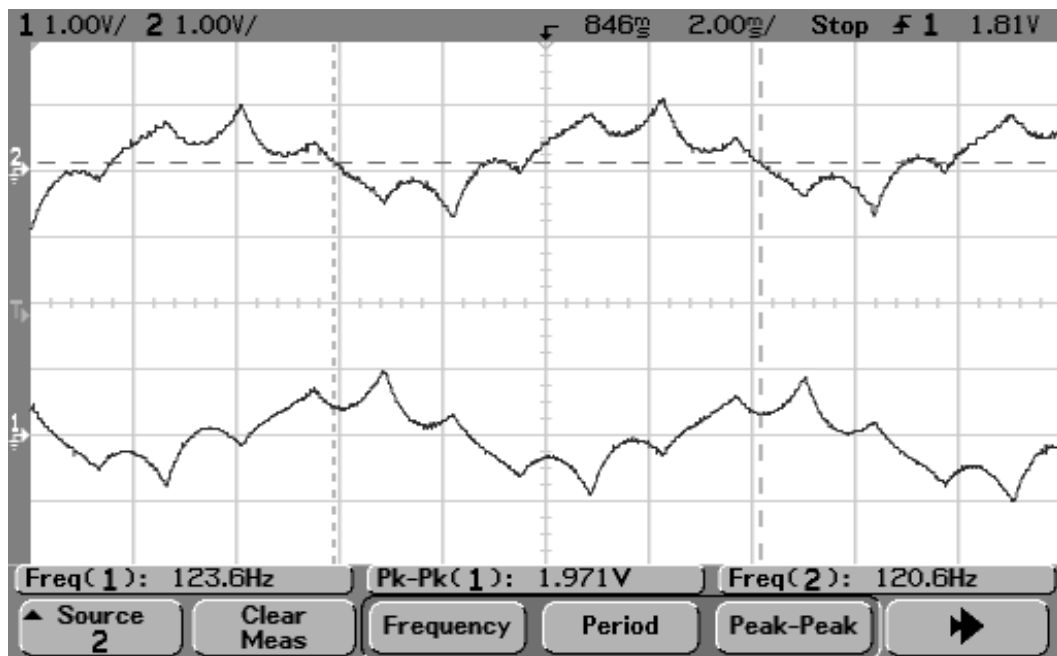


Figure 4.21: i_{s1} and i_{s2} waveforms for speed command of $2.25pu$ ($112.5Hz$)

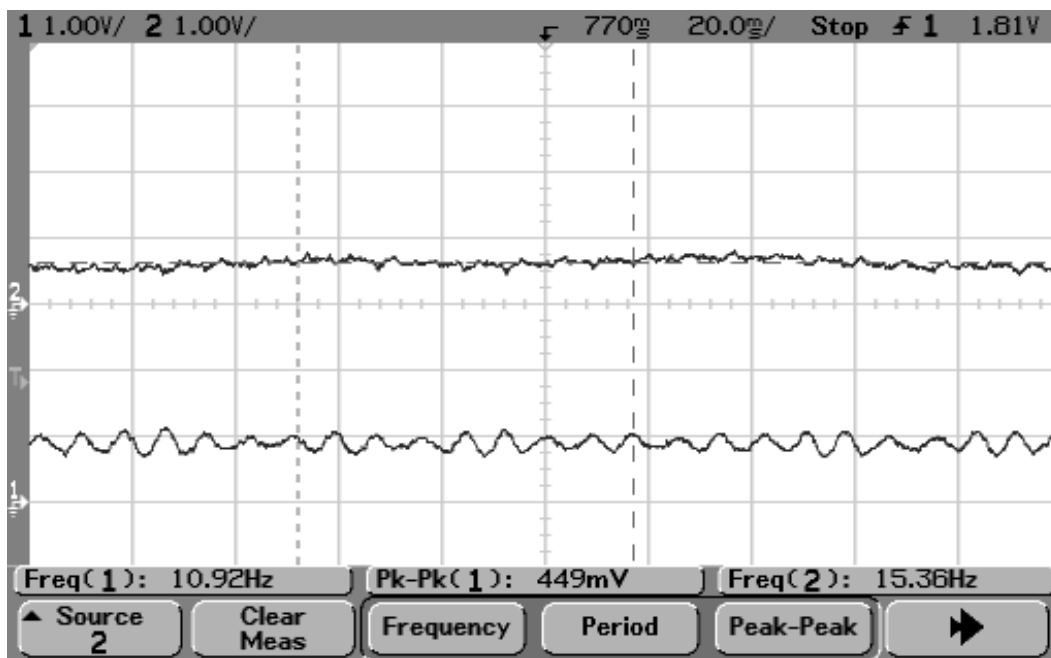


Figure 4.22: i_{sq} and i_{sd} waveforms for speed command of $2.25pu$ ($112.5Hz$)

Unit vectors $\cos\rho$ and $\sin\rho$,

Line currents i_{s1}, i_{s2} ,

Currents in (d,q) coordinate system i_{sd}, i_{sq} .

Case 1: Speed command changed from $0.75 pu$ (i.e., 37.5 Hz) to $1.5 pu$ (i.e., 75 Hz)

Refer Figs. 4.23, 4.24, 4.25, 4.26, 4.27, 4.28, 4.29

Case 2: Speed reversal from $1.25 pu$ (i.e., 62.5 Hz) to $-1.25pu$ (i.e., 62.5 Hz in reverse direction)

Refer Figs. 4.30, 4.31, 4.32, 4.33, 4.34, 4.35, 4.36.

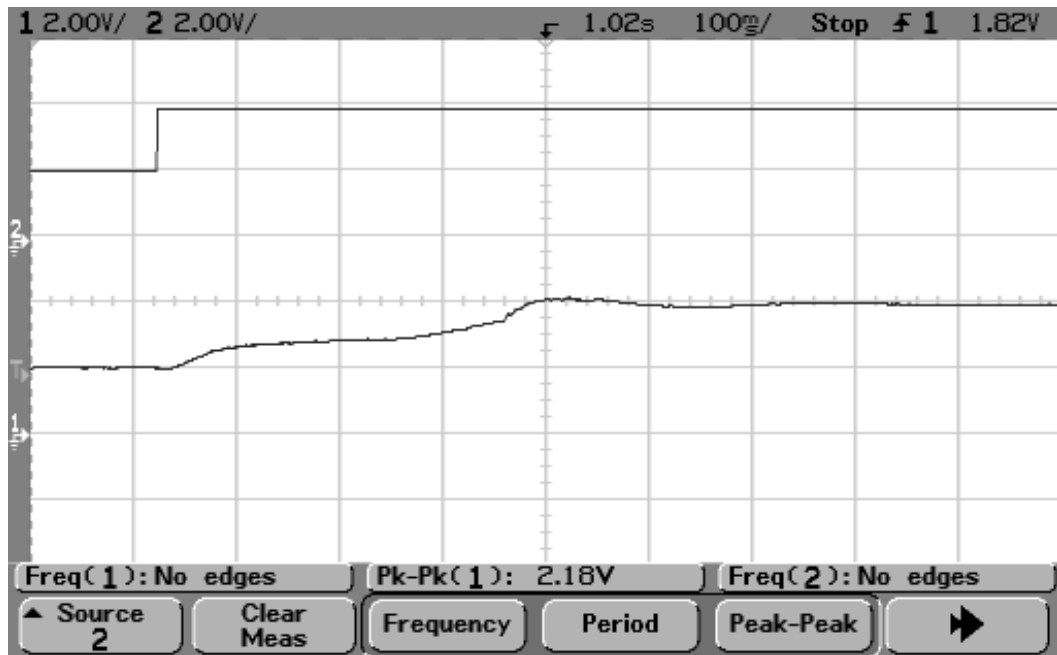


Figure 4.23: Rotor reference and actual speed during transition from 0.75 pu ($37.5Hz$) to 1.5 pu ($75Hz$)

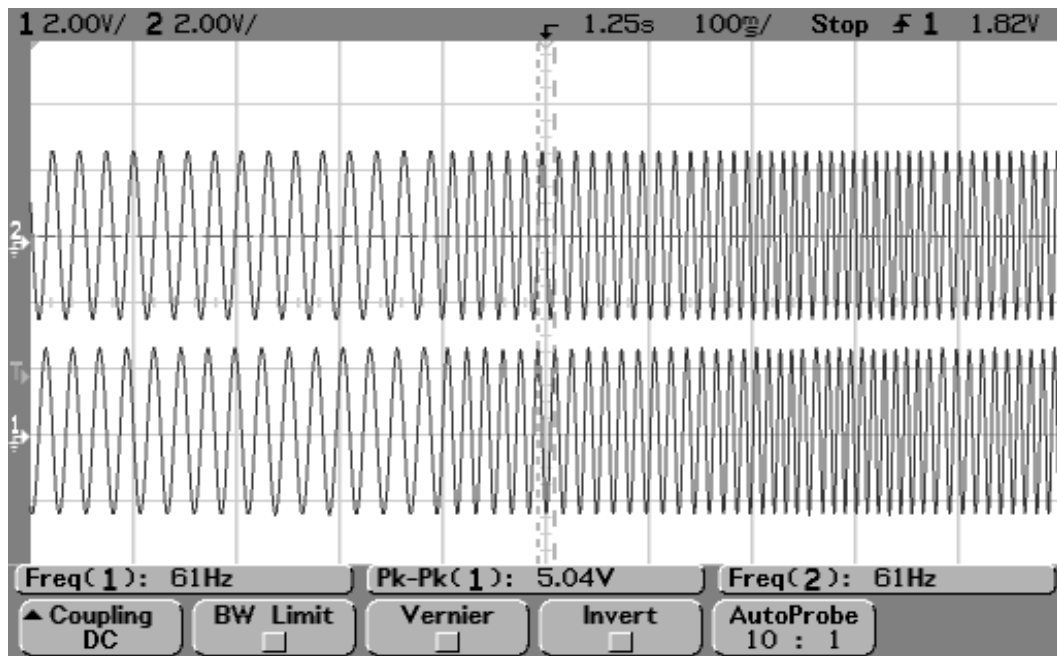


Figure 4.24: $\sin \rho$ and $\cos \rho$ during speed transition from 0.75 pu ($37.5Hz$) to 1.5 pu ($75Hz$)

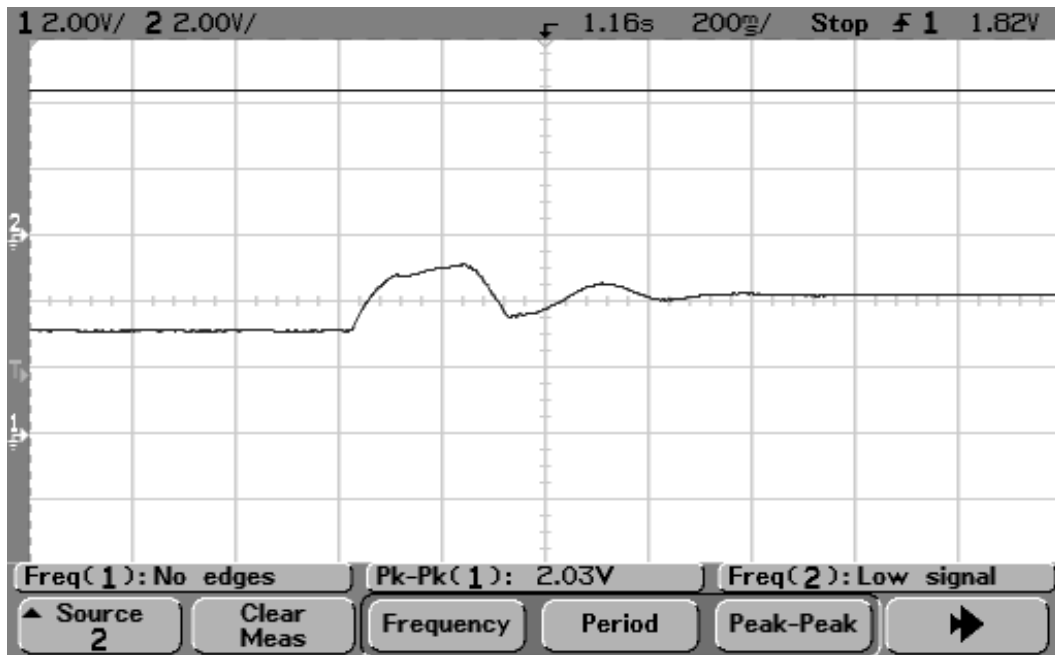


Figure 4.25: V_{max} and V_{dq} during speed transition from 0.75 pu (37.5Hz) to 1.5 pu (75Hz)

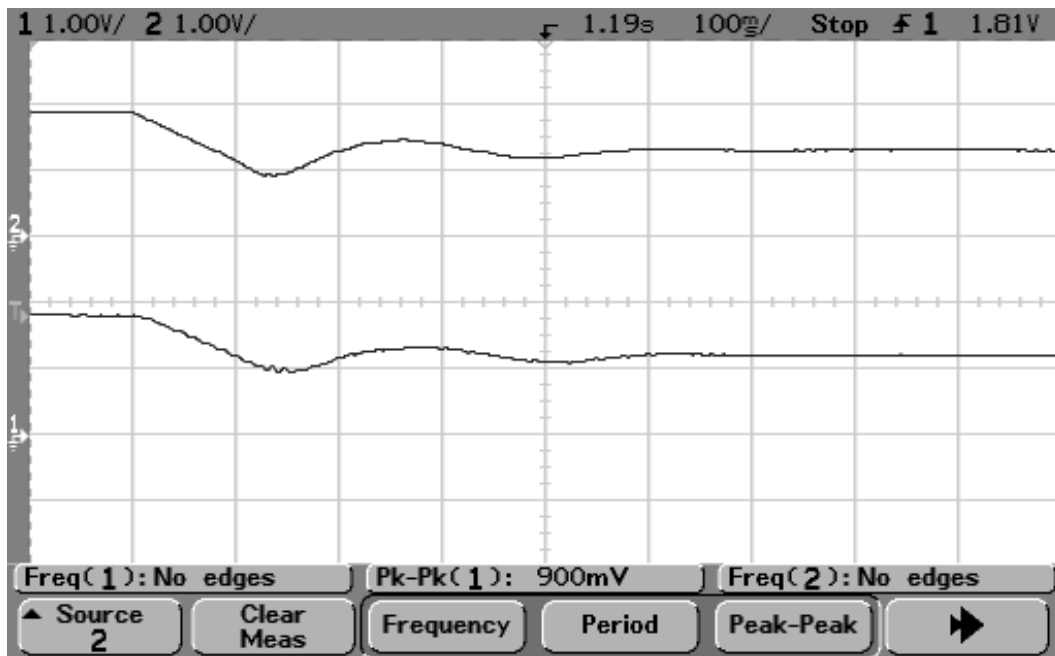


Figure 4.26: $i_{mr}(reference)$ and i_{mr} during speed transition from 0.75 pu (37.5Hz) to 1.5 pu (75Hz)

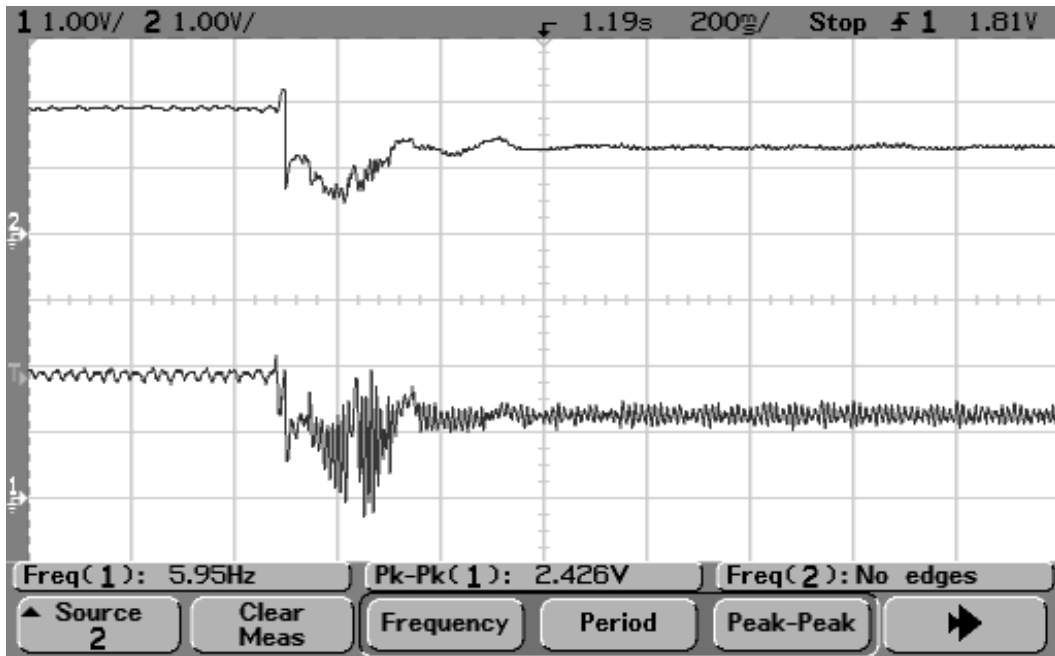


Figure 4.27: $i_{sd}(reference)$ and i_{sd} during speed transition from 0.75 pu (37.5Hz) to 1.5 pu (75Hz)

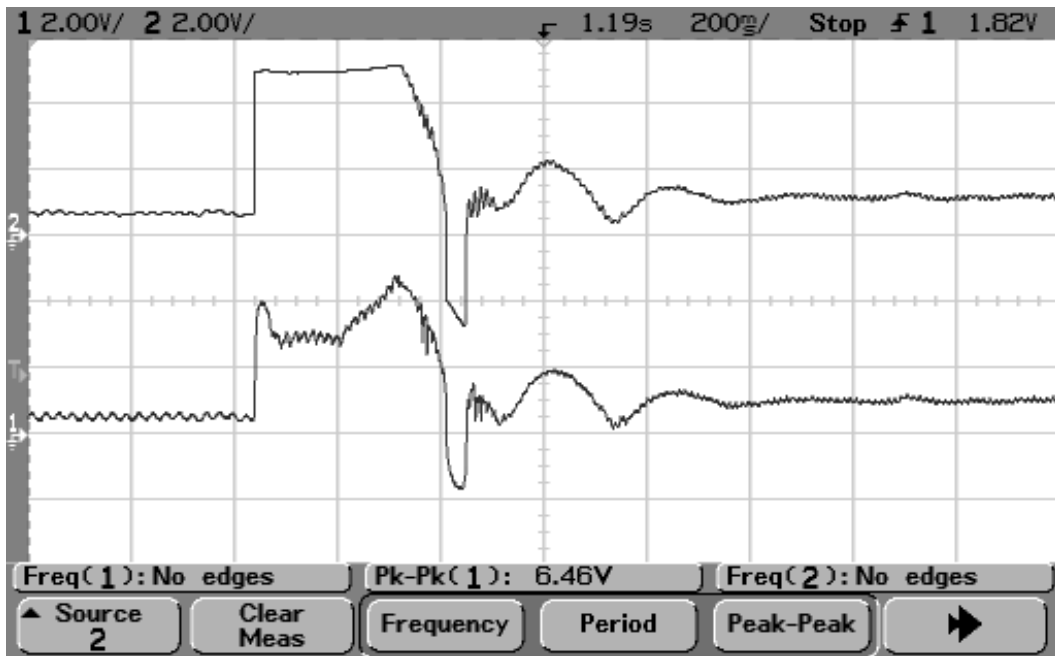


Figure 4.28: $i_{sq}(reference)$ and i_{sq} during speed transition from 0.75 pu (37.5Hz) to 1.5 pu (75Hz)

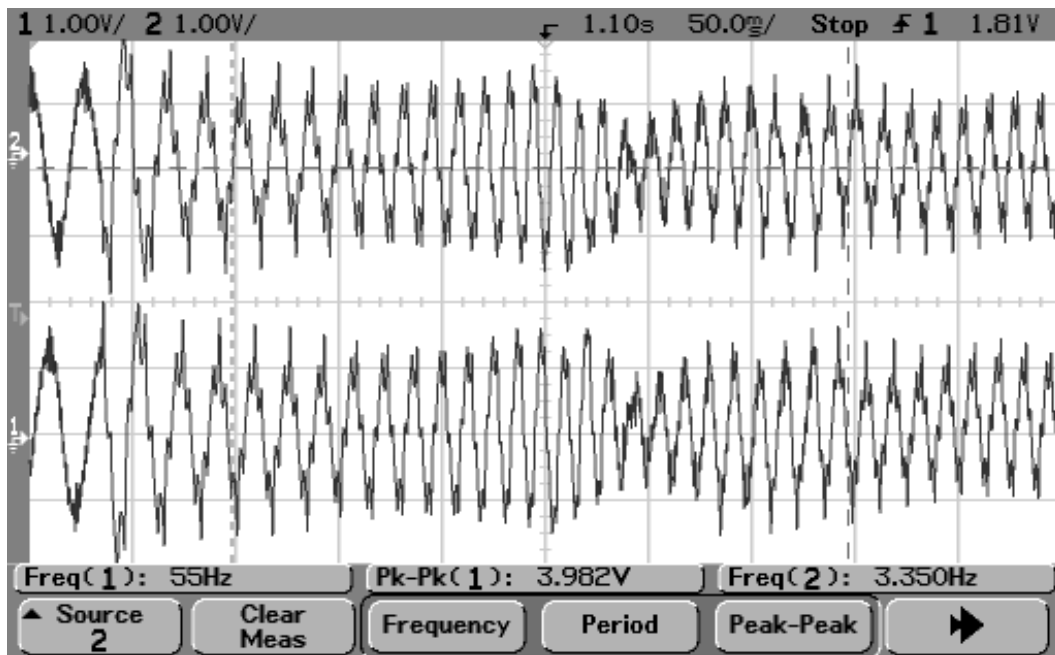


Figure 4.29: i_{s1} and i_{s2} during speed transition from 0.75 pu (37.5Hz) to 1.5 pu (75Hz)

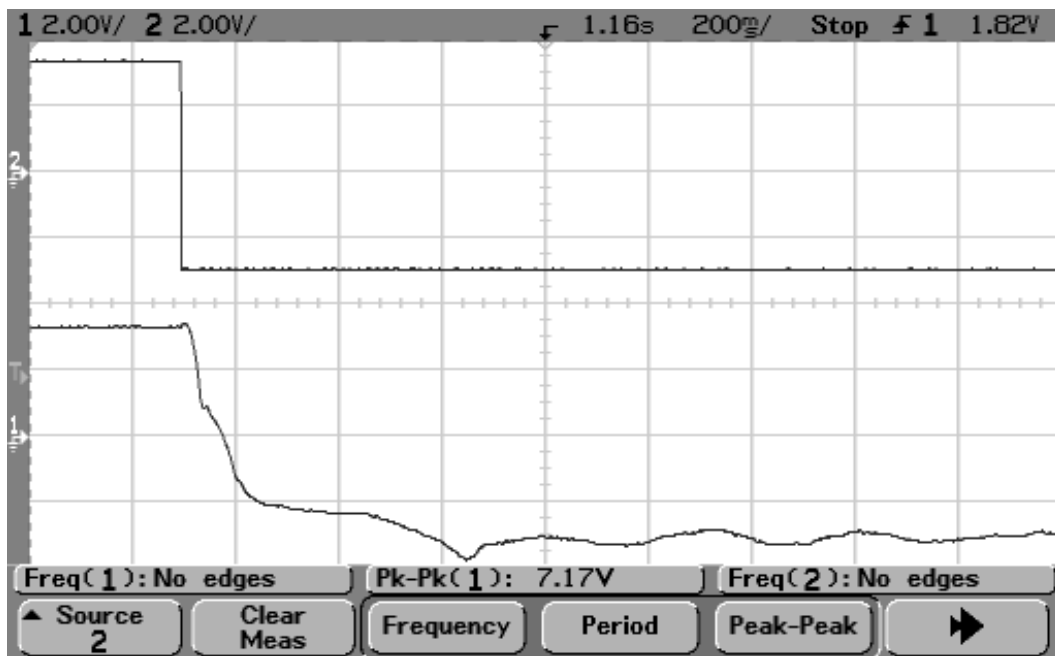


Figure 4.30: Rotor reference and actual speed waveform during the speed reversal from 1.25 pu to -1.25 pu

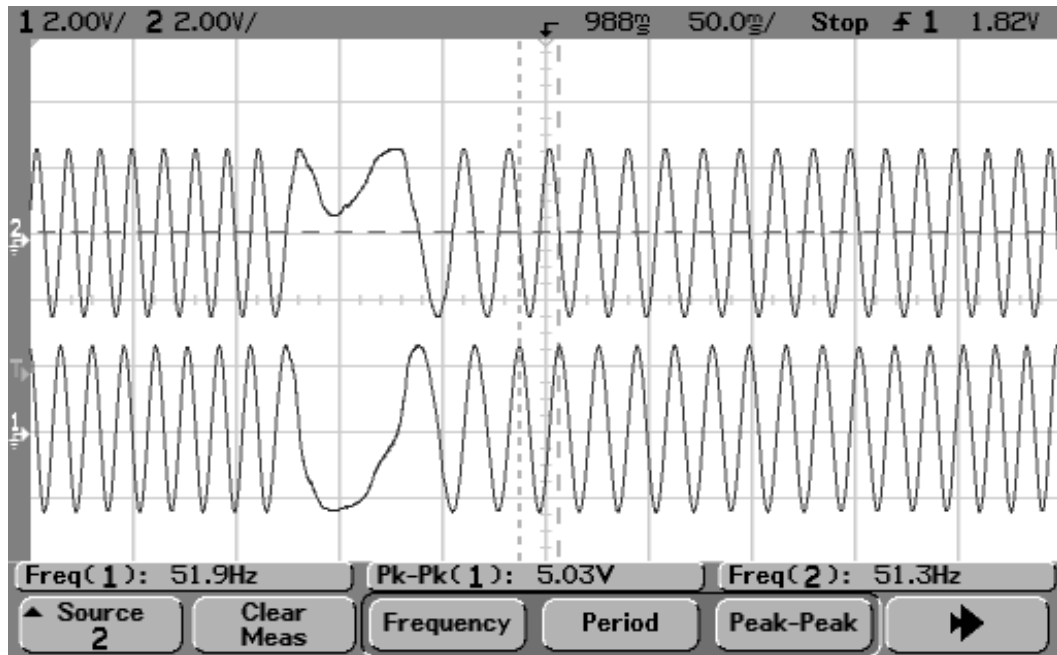


Figure 4.31: $\sin\rho$ and $\cos\rho$ waveform during the speed reversal from 1.25 pu to -1.25 pu

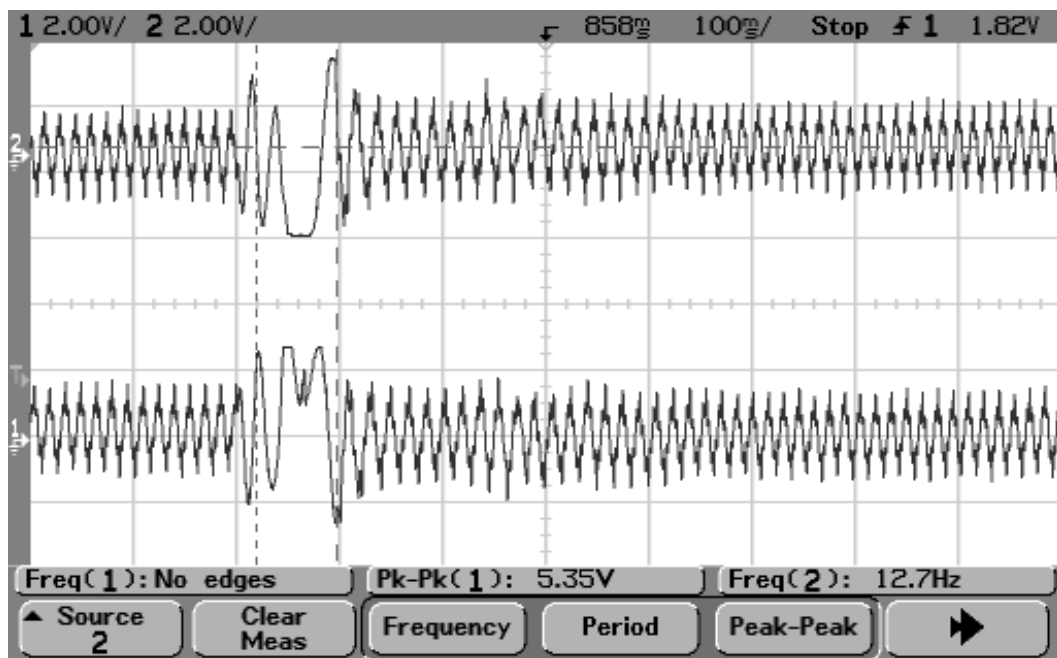


Figure 4.32: i_{s1} and i_{s2} waveform during the speed reversal from 1.25 pu to -1.25 pu

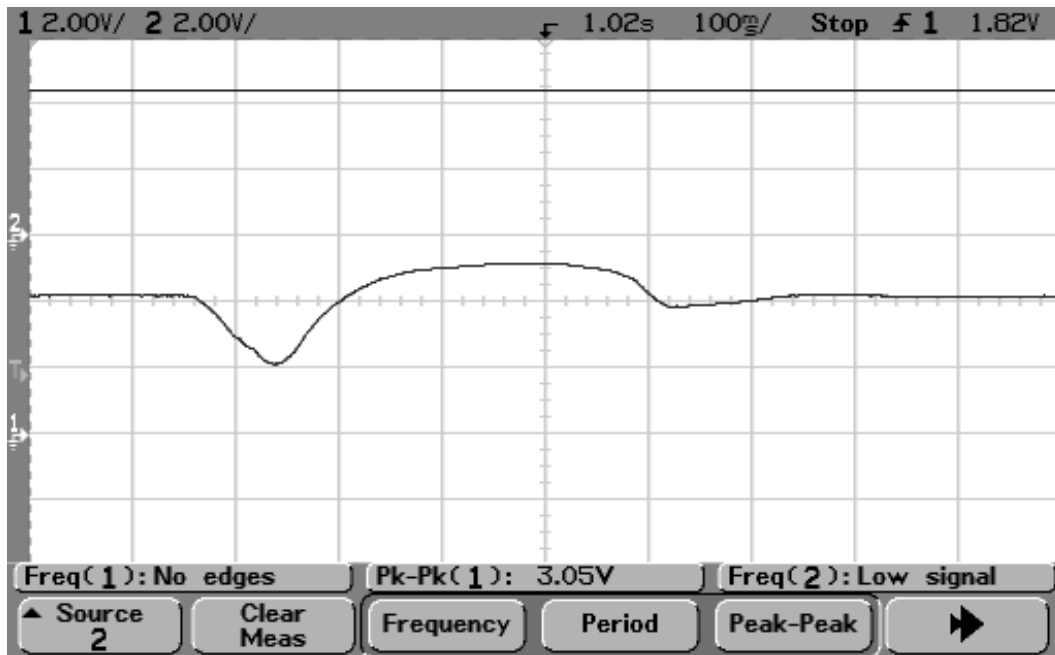


Figure 4.33: V_{max} and V_{dq} waveform during the speed reversal from 1.25 pu to -1.25 pu

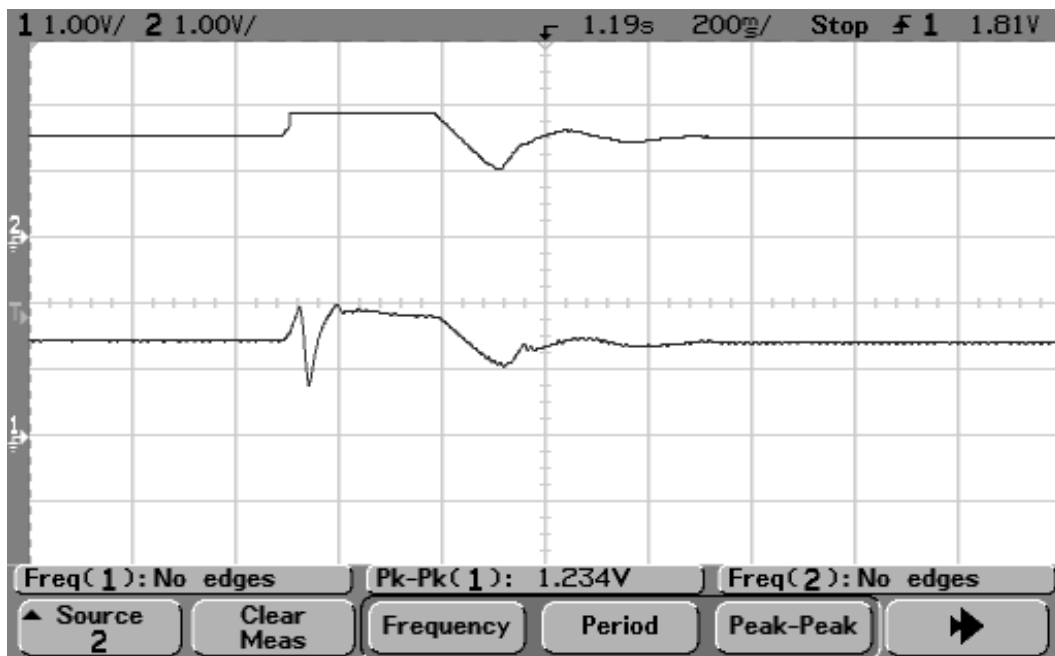


Figure 4.34: $i_{mr}(reference)$ and i_{mr} waveform during the speed reversal from 1.25 pu to -1.25 pu

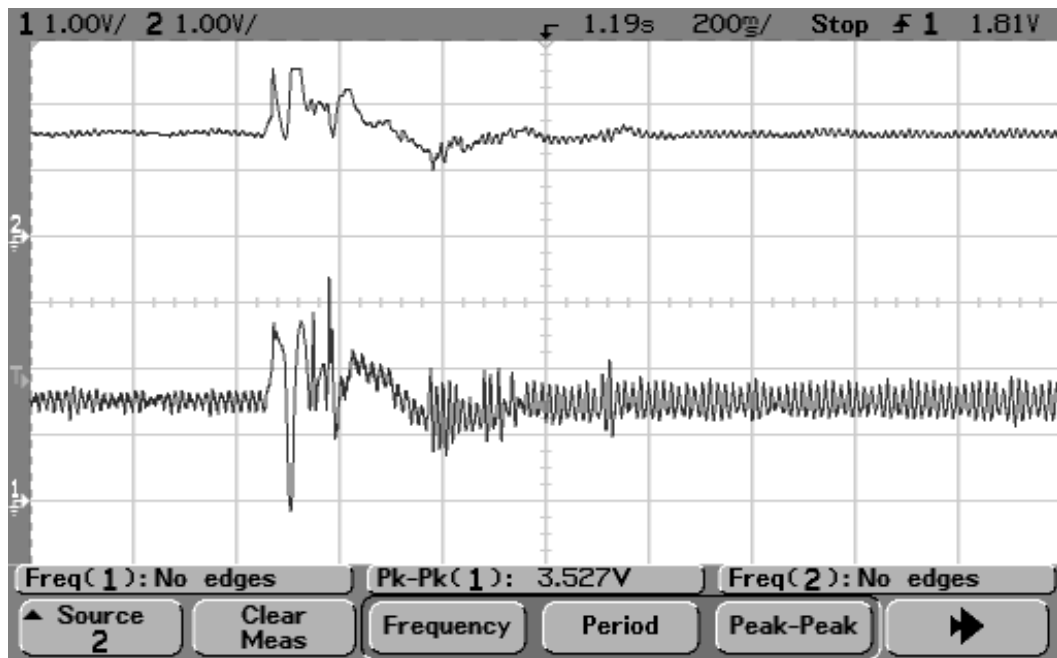


Figure 4.35: $i_{sd}(reference)$ and i_{sd} waveform during the speed reversal from 1.25 pu to -1.25 pu

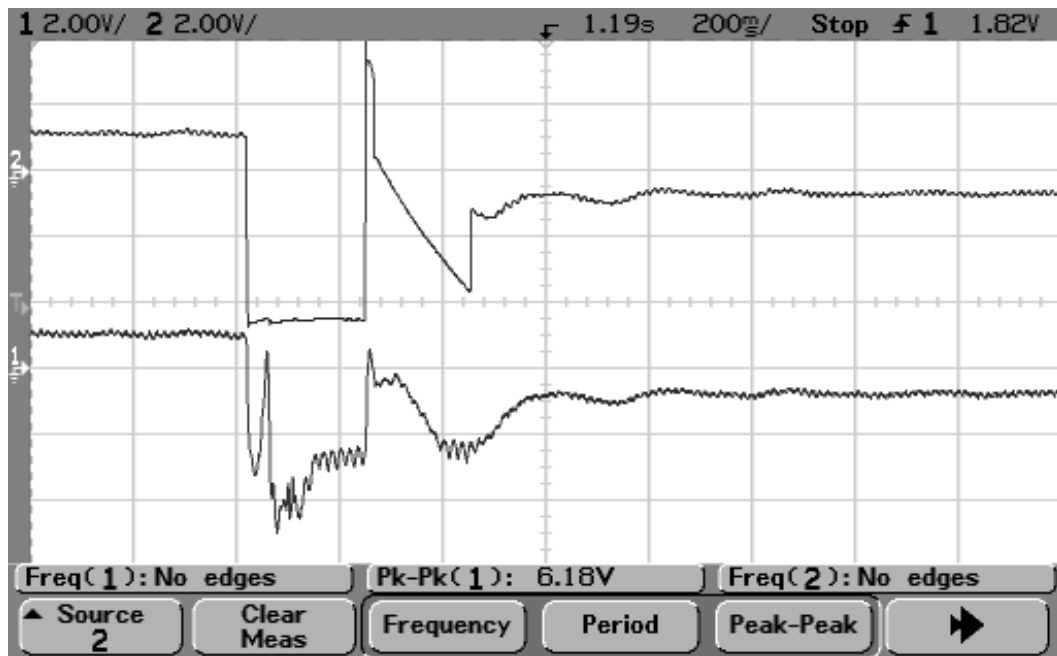
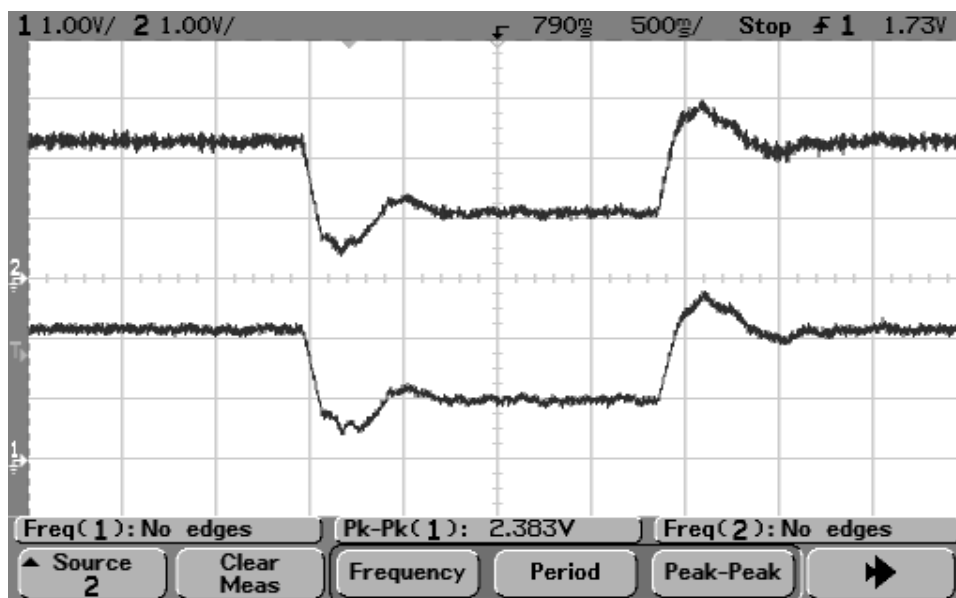


Figure 4.36: $i_{sq}(reference)$ and i_{sq} waveform during the speed reversal from 1.25 pu to -1.25 pu

VOLTAGE	220 V
CURRENT	2.5 A
POWER	0.55 KW
POLES	4
SPEED	1500 rpm

Table 4.1: Details of the induction motor-2

Figure 4.37: $i_{sq}(reference)$ and i_{sq} for speed command 1.25 pu (62.5 Hz) and load 129.2W

4.6 Machine-2 Loading Waveforms

For loading purpose one IM-DG set has been used. Parameters are given in this table 4.1.

Two transients of unloading and loading are captured in the waveforms 4.37 and 4.38.

4.7 Conclusion

The performance of the proposed scheme under steady state as well as during the transients are presented. A good dynamic performance of the drive is observed under both load changes and changes in reference speed. Performance in six-step mode is also very good. In an actual

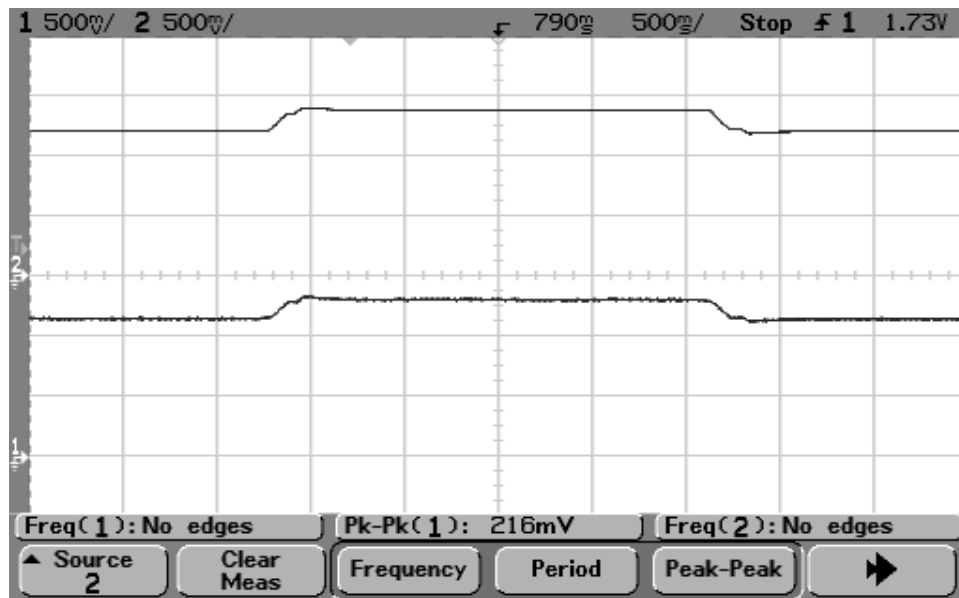


Figure 4.38: $i_{mr}(reference)$ and i_{mr} for speed command 1.25 pu (62.5 Hz) and load 129.2W

traction system, most of the time, motor will be operating in field weakening mode. So six-step steady state performance is required to be good enough. Some important points are mentioned here.

1. Controller parameters calculated are found to be faster so they have been slowed by tuning.
2. K value in sensorless algorithm which is found by tuning, is nearly same in simulation and experimental program.
3. V_{dc} is uncontrolled here and during transients starts fluctuating. This hampers the transient performance.
4. If algorithms are implemented on 20-bit representation and ADC is of higher bits, performance will certainly improve.
5. In overmodulation mode prior to six-step, subharmonics get generated as switching frequency is 770Hz(low) so carrier frequency can be increased for that region but this requires a hysteresis band for stability and for certain speed range inverter will be switching at high rate.

References

- [1] Vikram Kaura, “ A New Method To Linearize Any Triangle Comparison Based PWM By Reshaping The Modulation Command ”,IEEE transactions on Industry Applications, Volume 33, NO.5, September/October 1997, Pages 1254-1259.
- [2] Ashwin M. Khambadkone,“ Compensated Synchronous PI current controller in Overmodulation range and Six-step Operation of Space-Vector-Modulation Based Vector Controlled Drives ”,IEEE transactions on Industrial Electronics, Volume 49, NO.3, June 2002, Pages 574-580.
- [3] Sang-Hoon Kim,“ Maximum Torque Control of an Induction Machine in the Field-Weakening Region ”,IEEE transactions on Industrial Electronics, Volume 31, NO.4, July/August 1995, Pages 787-794.
- [4] Werner Leonhard, “Control of Electric Drives”, Springer-Verlag Berlin, Heidelberg, 1985.
- [5] V.T. Ranganathan ,“Field Oriented Control of AC drives”, Lecture notes of Electric Drives, IISc Bangalore.
- [6] B. Srinivas Rao, “DSP based sensorless vector control of induction motor”, M.E. thesis, EE Dept, IISc, Bangalore, January 2003.
- [7] S. Venugopal, “Study on Overmodulation Methods for PWM INVERTER Fed AC DRIVES”, M.Sc. thesis, EE Dept, IISc, Bangalore, May 2006.
- [8] N. Praveen Kumar, “FPGA based sensorless vector control of induction motor”, M.E. thesis, EE Dept, IISc, Bangalore, July 2006.